NMR Investigations of Peptide-Membrane Interactions, Modulation of Peptide-Lipid Interaction as a Switch in Signaling across the Lipid Bilayer

Licentiate thesis

Sofia Unnerståle

Department of Biochemistry and Biophysics
Stockholm University
2010

NMR Investigations of Peptide-Membrane Interactions,

Modulation of Peptide-Lipid Interaction as a Switch in Signaling across the Lipid Bilayer

The complexity of multi cellular organisms demands systems that facilitate communication between cells. The neurons in our brains for instance are specialized in this cell-cell communication. The flow of ions, through their different ion channels, across the membrane, is responsible for almost all of the communication between neurons in the brain by changing the neurons membrane potentials. Voltage-gated ion channels open when a certain threshold potential is reached. This change in membrane potential is detected by voltage-sensors in the ion channels. In this licentiate thesis the *Homo sapiens* voltage- and calcium-gated BK potassium channel (HsapBK) has been studied. The NMR solution structure of the voltage-sensor of HsapBK was solved to shed light upon the voltage-gating in these channels. Structures of other voltage-gated potassium channels (K_v) have been determined by other groups, enabling comparison among different types of K_v channels. Interestingly, the peptide-lipid interactions of the voltage-sensor in HsapBK are crucial for its mechanism of action.

Uni cellular organisms need to sense their environment too, to be able to move towards more favorable areas and from less favorable ones, and to adapt their gene profiles to current circumstances. This is accomplished by the two-component system, comprising a sensor protein and a response regulator. The sensor protein transfers signals across the membrane to the cytoplasm. Many sensor proteins contain a HAMP domain close to the membrane that is involved in transmitting the signal. The mechanism of this transfer is not yet revealed. Our studies show that HAMP domains can be divided into two groups based on the membrane interaction of their AS1 segments. Further, these two groups are suggested to work by different mechanisms; one membrane-dependent and one membrane-independent mechanism.

Both the voltage-gating mechanism and the signal transduction carried out by HAMP domains in the membrane-dependent group, demand peptide-lipid interactions that can be readily modulated. This modulation enables movement of peptides within membranes or within the lipid-water interface. These conditions make these peptides especially suitable for NMR studies.

TABLE OF CONTENTS

ABBREVIATIONS

Af	*Archaeoglobus fuldigus*
AS	amphiphilic segment
BK channel	Big K^+ channel, MaxiK channel (*Slo1* in *Drosophila melanogaster*)
BMRB	biological magnetic resonance data bank
CD	circular dichroism
$CHCl_3$	chloroform
CH_3OH	ethanol
CMC	critical micelle concentration
COSY	correlation spectroscopy
DHPC	1,2-dihexanoyl-sn-glycero-3-phosphocholine
DMPC	1,2-dimyristoyl-sn-glycero-3-phosphocholine
DMPG	1,2-dimyristoyl-sn-glycero-3-phospho-(1'-rac-glycerol)
DPC	dodecylphosphocholine
$GdCl_3$	guadiniumchloride
HAMP	Histidine kinases, Adenylyl cyclases, Methylaccepting proteins and other Prokaryotic signaling proteins
H^{α}	alpha proton
H^N	amide proton
HsapBK	*Homo sapiens* BK
K_{ir}	Inwardly rectifying potassium channel
K_v	voltage-gated potassium channel
K_vAP	voltage-gated potassium channel from the archeabacterium *Aeropyrum Pernix*
LUV	large unilamellar vesicle
MCP	methyl-accepting chemotaxis proteins
NaPi	sodium phosphate
Na_v	voltage-gated sodium channel
NMR	nuclear magnetic resonance
NOE	nuclear Overhauser effect
NOESY	nuclear Overhauser effect spectroscopy
PDB	protein databank
PFG	pulse field gradient
POPC	1-palmitoyl-2-oleoyl-*sn*-glycero-3-phosphocholine
POPG	1-palmitoyl-2-oleoyl-*sn*-glycero-3-phospho-(1'-rac-glycerol)
S1	segment 1
TOCSY	total correlation spectroscopy
TM2	transmembrane helix 2
τ_{mix}	mixing time

ORIGINAL PAPERS

This licentiate thesis is a summary of the following papers, which will be referred to in the text by their Roman numerals.

I. Unnerståle S, Lind J, Papadopoulos E and Mäler L. *Solution Structure of the HsapBK K^+ Channel Voltage-Sensor Paddle Sequence* (2009) Biochemistry 48, 5813-5821

II. Unnerståle S, von Heijne G, Draheim R.R and Mäler L. *Membrane-based Induction of α-helical structure within a subset of peptides derived from HAMP domains* (submitted)

1. SIGNALING ACROSS THE MEMBRANE

The cell membrane is essential for the compartmentalization defining the cell. However, this compartmentalization creates a requirement of signaling across the cell membrane. There are different methods to get messages across a membrane. The most specific ones involve integral membrane proteins. The flow of sodium (Na^+), potassium (K^+), calcium (Ca^{2+}) and chloride (Cl^-) ions across the cell membrane, by the means of their different transport proteins, play fundamental roles in the functioning of nerve cells by affecting the cell membrane potential. Ion transport is mediated by for instance voltage- and ligand-gated ion channels. Regarding voltage-gated ion channels, it is not completely understood how a change in membrane potential changes their open probability (Section 1.1). Further, even uni cellular organisms need to sense their environment, to find food and flee from harm. This is mediated by the two-component system (Section 1.3), which is well studied. However these systems comprise many modular domains, whose mechanisms are not yet revealed (Section 1.4).

1.1 VOLTAGE-GATED ION CHANNELS – COMMUNICATION IN EXCITABLE CELLS

Voltage dependent ion channels are crucial for the information transfer in excitable cells (1). When the cell membrane of an excitable cell is at rest i.e. is not stimulated, the voltage across the cell membrane adopts a specific value known as the resting potential. This potential arises because the membrane is differently permeable to different ions, depending on the state, number and single-channel conductance of the ion channels transporting that particular ion; and ions are distributed unequally across the membrane, due to active transport by pumps and other carrier proteins, creating electro-chemical gradients. When a threshold potential specific for each channel type is reached, the open probability of that voltage-gated ion channel increases. The change in membrane potential is detected by an arginine-rich motif (2, 3, 4) which is a common motif to members of the S4 superfamily of K^+, Na^+ and Ca^{2+} channels, resulting in a movement of these gating charges (5). As a result, the channel pore opens more frequently. Upon channel opening, ions flow across the membrane leading to further signaling by influencing other electro-chemical gradients and gating charges.

The potassium channels are the most ancient ion channels, from which Na^+ and Ca^{2+} channels have been developed. All potassium channels are tetrameric integral membrane proteins forming aqueous pores in which K^+ can flow with its electro-chemical gradient (6). Voltage-gated potassium channels (K_v) are the representative members of the S4 superfamily. They comprise six transmembrane segments a subunit, where S1-S4 constitutes the voltage sensor domain; and S5-S6, and the pore-forming loop in

between them, constitutes the pore domain. The sodium and calcium channels resemble the potassium channel (7) with the distinction that they comprise one sole subunit constituting four six-transmembrane helix domains. The K_v channels are the most diverse voltage dependent ion channels (6). At least 18 genes for K_v α-subunits are known to be expressed in mammalian cells. These genes are divided in six different subfamilies: K_v1.1-1.7 (corresponding to *Shaker* in *Drosophila*), K_v2.1 and K_v2.2, K_v3.1-3.4, HERG and Maxi K (8).

1.2 A Voltage- and Ca^{2+}-Activated Potassium Channel

Maxi K or Big K^+ (BK) channels are activated by both depolarization and an increase in intracellular calcium levels, providing a possibility to integrate electrical signals in the cell with signaling cascades involving Ca^{2+} i.e. metabolic signals. A depolarization of the membrane can activate BK channels in the absence of Ca^{2+} (9), suggesting that the two mechanisms can act independently. BK channels are characterized by a large conductance (10), hence the name; nevertheless they are surprisingly potassium specific. The core topology of the α-subunit of the K_v channels is preserved in the α-subunit of BK channels (Fig. 1). However, an extra transmembrane segment is found N-terminally, resulting in seven transmembrane domains (S0-S6) and an extracellular N-terminus (11, 12). The extra transmembrane segment allows modulation of the Ca^{2+} sensitivity by the regulatory β-subunit, which comprises two transmembrane segments and a large extracellular loop (11). In K_v channels, on the other hand, β-subunits are intracellular proteins that modulate inactivation (8). Further, a large cytosolic domain (S7-S10) is found C-terminally of the BK channels. This domain consist of a regulator of conductance for potassium (RCK) domain (13) and the calcium sensing tail-domain (14). The conserved charged residues in the S4 domain are found also in BK channels, and in addition gating charge is also found in the S3 domain (15).

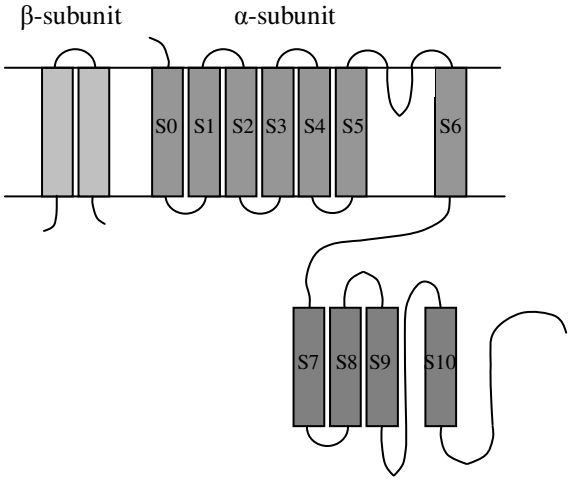

Fig. 1. Membrane topology of the BK channel. The α-subunit is similar to K_v channels in many aspects, but contains seven transmembrane helices (S0-S6) instead of six. The channel also features a large cytoplasmic domain (S7-S10), which is not found in K_v channels.

1.3 The Sensing Proteins of the Two-component Systems Transmit Signals across the Membrane in *E. coli*

Environmental adaption can be immediate and is in fact crucial in gene regulation for

even the most basic organisms to survive. The environment is constantly changing and hence prokaryotes need to adapt their gene expression profiles and their regulation of gene product activity to match current circumstances. The main system used by bacteria for this task is the two-component signal transduction system, which comprises a sensing protein and a response regulator (Fig. 2) (16, 17, 18). The sensing protein senses the environment predominantly through ligand binding. These proteins are often transmembrane, and hence transmit the signal across the lipid bilayer, often leading to autophosphorylation on the cytosolic part of the protein (19). Consequently, the signal will change the phosphorylation state of the response regulator. There are different types of prokaryotic sensing proteins i.e. sensor histidine kinases (SKs) and methyl-accepting chemotaxis proteins (MCPs) (20).

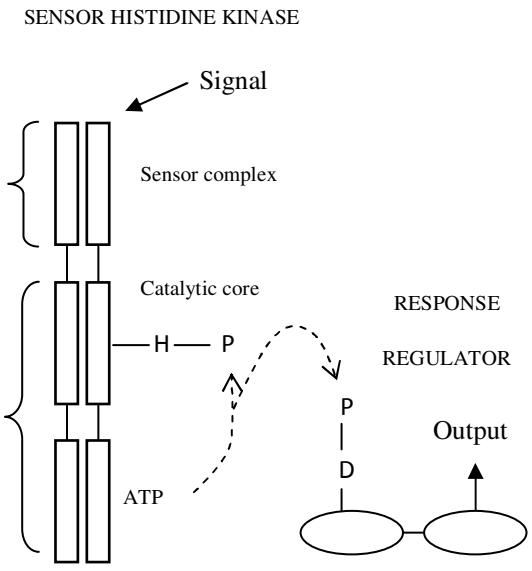

Fig. 2. The sensor protein and the response regulator of the two-component system. Here the sensor protein is represented by a sensor histidine kinase. Upon stimuli, the sensor histidine kinase autophosphorylates on a conserved histidine residue. The phosphoryl group is transferred to an aspartate residue on the response regulator, which initiates further signal transduction.

The response regulators corresponding to SKs usually bind DNA operators or activating sites, and hence influence the gene expression. In the *E.coli* K-12 genome 27 membrane bound sensors have been identified (20) including $NarX_{Ec}$ and $EnvZ_{Ec}$. $NarX_{Ec}$ (21) senses nitrate and nitrite and initiates a signaling cascade which increases gene expression of genes involved in nitrate respiration, so that nitrate can be utilized as an electron acceptor under anaerobic conditions. Concurrently the expression of genes involved in other respiratory pathways is repressed by the same signal cascade. $EnvZ_{Ec}$ (22, 23), on the other hand, is involved in adaption to changes in osmolarity (24).

MCPs, on the contrary, regulate response regulators in a cascade that ultimately affects the flagellar rotation of flagellar bacteria, providing the ability of movement in a temporal gradient towards attractants and away from repellants (25, 26). This process in which flagellar rotation is changed between continues movement in the same direction, and tumbling, leading to a biased random walk, is known as bacterial chemotaxis. In *E.coli* five membrane spanning MCPs are found, among which Tar_{Ec} is the most studied (27). Tar_{Ec} senses the attractants aspartate and maltose and the repellants cobalt and nickel.

A linker domain is found in many prokaryotic transmembrane signal transduction proteins, i.e. in 15 of the 27 known membrane bound *E.coli* histidine kinases and in all *E.coli* MCPs (28), connecting the signal input domain with the catalytic auto-phosphorylation core (Fig. 3). It is most frequently located close to the membrane on the cytosolic side, C-terminal to a transmembrane helix. This linker domain is known as the HAMP-domain, since it is found in Histidine kinases, Adenylyl cyclases, Methylaccepting proteins and other Prokaryotic signaling proteins (28). The signal transduction of prokaryotes is well studied, but nevertheless, the mechanism of the HAMP-domain transmitting the signal remains unknown.

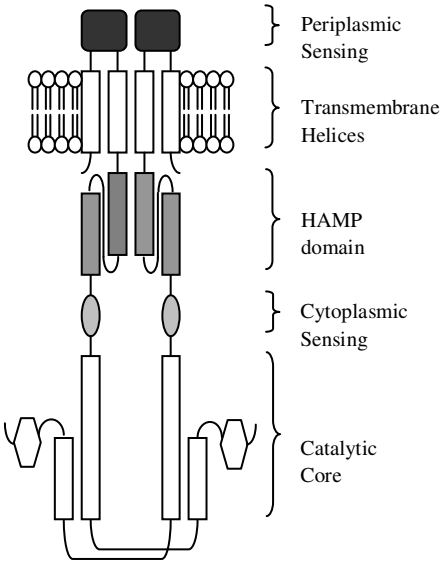

Fig. 3. Location of the HAMP-domain in a sensor histidine kinase. The sensor histidine kinase comprises the sensing domain and the catalytic core. The periplasmic sensing domain receives the signal and transmits it to the cytoplasmic sensing domain via four transmembrane helices and the HAMP domain. The mechanism that transmits the signal is not yet revealed.

1.4 HAMP-DOMAINS IN SENSOR PROTEINS

Cysteine and disulfide scanning of the HAMP-domain has shown that it consist of two amphiphilic segments (AS1 and AS2), predicted to be helices, and a middle segment, connecting the two helices (29). The helical amphipathicity in AS1 and AS2 is conserved among HAMP-domains, while the primary structure is not (20), suggesting that amphipathicity is a crucial property for their mechanism of action. Several mechanisms for HAMP-domain function are proposed. The gearbox model, for instance, suggests a 26 degree structural re-arrangement from the unusual x-da configuration seen in the solution structure of Af1503 into an a-d packing configuration (30). The helix interaction model, on the other hand, suggests that the amphipathic helices interact with the membrane and that this interaction can be modulated (20). In this model, in contrary to the gearbox model, the membrane is a structural component in the transmembrane signal transduction. It seems plausible, that different HAMP domains use different signal transduction mechanisms.

2. Interactions between Peptides and Lipids Studied by NMR

Spectroscopy is the study of the interaction between electromagnetic radiation and matter. In nuclear magnetic resonance (NMR) spectroscopy the interaction of electromagnetic radiation in the radio-frequency portion of the electromagnetic spectrum and molecules are studied. NMR is the spectroscopic method that gives the most detailed information about molecules i.e. atomic resolution. First, a general introduction to NMR is presented (Section 2.1). Second, the specific challenges arising in the study of membrane proteins are discussed (Section 2.2.) as well as the NMR experiments suitable for these studies (Section 2.3-2.4).

2.1. Nuclear Magnetic Resonance Spectroscopy: A General Introduction

2.1.1. The Nuclear Spin, or What is Measured in NMR Experiments?

Some nuclei have got an intrinsic property that is called the spin angular momentum ($\bar{I}$). This is a phenomenon that is hard to grasp, especially since there is no macroscopic counterpart. One can think of it though as an angular momentum, which is the vector perpendicular to the orbit of a particle that is rotating in a circular plane. However, the peculiar part is that the nucleus does not rotate! None the less, the nuclei thus have a spin angular momentum, and in fact its building blocks have got this property too. The nucleus consists of neutrons and protons, which each have a spin quantum number of one half, we call them spin-1/2 particles. Further, neutrons and protons are built up of three quarks each, and quarks themselves are spin-1/2 particles too. In the ground state, two of these quarks will arrange themselves anti parallel and cancel out; hence, the resulting spin of the neutron and the proton is spin-1/2. The spin quantum number (I) of a nucleus will thus depend on the numbers of neutrons and protons that build up the nucleus.

The hydrogen nucleus is a spin-1/2 nucleus since it consists of a single proton. Associated with the spin angular momentum is a magnetic momentum ($\bar{u}=\gamma\bar{I}$). The strength of this little magnet is described by the gyromagnetic ratio (γ), which is a constant specific for each nucleus. The orientation of the spin angular momentum in space is quantized, i.e. it adopts specific orientations, and hence the magnetic momentum is quantized too. In a magnetic field this gives rise to the Zeeman levels (m), which are two for a single spin-1/2 nucleus (2I+1). These two Zeeman levels are called the alpha state and the beta state. For protons the alpha state is the spin up state and the beta state is the spin down state, due to the positive gyromagnetic ratio. The frequency that corresponds to the gap between these two levels is called the Larmor frequency (ω_0) and is what is measured in an NMR experiment.

2.1.2. Chemical Shifts, or Why Nuclei in Different Environment Precess with Different Frequencies

If all of the protons in for instance a peptide would have the same Larmor frequency, not much could be read out from the experiment. One would simply get a large proton signal proportional to the amount of protons in the sample. Luckily, the chemical shift is dependent on the local environment of each proton. This is due to that electrons have a spin angular momentum too and hence a magnetic moment. These little magnets will affect the Larmor frequency of the spin of nearby nuclei. Moreover, nuclei with magnetic moments will affect other magnetic nuclei in their close vicinity. Hence the local environment around each proton will affect the energy separation between the energy levels of that particular spin, leading to different Larmor frequencies.

The structure of an amino acid provides an ideal target for NMR measurements, since the amide proton, the alpha proton and the side chain protons are surrounded by different environments, and thus appear at distinct positions in the NMR spectrum (Fig. 4). For instance, the amide protons (H^N) will appear around 8 ppm, the alpha protons (H^α) around 4 ppm and the methyl group protons in alanine, valine, leucine or isoleucine will have chemical shifts around 1 ppm (31).

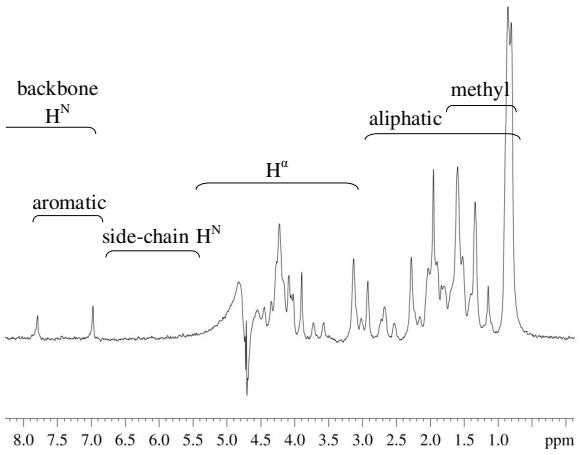

Fig. 4. The different protons in an amino acid will precess with different frequencies, since they exhibit different local environments. Here a 1D spectrum of AS1p-Env$_{Ec}$ in phosphate buffer is depicted. Backbone H^N and side-chain H^N are not seen because the sample is dissolved in D_2O to avoid severe baseline distortions originating from the water signal. Aromatic side-chains are seen around 7 pp, H^α around 4 ppm, aliphatic side-chains have a broad chemical shift range and methyl protons are found around 1 ppm. Here HD2 and HE1 of H191 are seen in the aromatic region.

2.1.3. The Bulk Magnetization: the Sum of the Spins in the Sample

That the spin angular momentum is quantized does not mean that all of the spins point either up or down; due to superposition states the spin consists of one alpha and one beta part. However, in a magnetic field the state where the spin is aligned with the magnetic field will be energetically more favored. This will lead to a slight increase of spins in the alpha state, the bulk equilibrium magnetization. The preference for the alpha state is very small though, because the thermal energy in the sample favors a random distribution of spins and is much larger in magnitude.

When a sample is put in a magnetic field it will take some time to build up the bulk equilibrium magnetization. When the bulk magnetization is aligned along the z-axis, the equilibrium state, it is hard to measure the signal from the nuclei with different environments, because the static magnetic field is enormous and in the same direction as the magnetization vector. To circumvent this problem non-equilibrium states have to be created.

2.1.4. The Pulsed-Field NMR Experiment, or How to Extract Information from the Spin Nuclear Angular Momentum

In the NMR experiment non-equilibrium states are produced by displacing the bulk magnetization from the z-axis, by the means of a burst of radiofrequency electromagnetic radiation, a pulse. The pulse comes from a coil perpendicular to the z-axis (32) and oscillates with a radiofrequency close to the Larmor frequency, for instance 600 MHz for ^{1}H spins in a magnetic field of 14.1 Tesla. When displaced from the magnetic field the magnetization vector starts to precess around the z-axis with the Larmor frequency, as a consequence of that it is in a great magnetic field, slowly relaxing back to equilibrium, to retain the Boltzman distribution of the spin-states. Beta states are thus flipping back to the alpha state, and energy is given to the surrounding that is in thermal equilibrium, and thus the flow of energy to the surrounding is much more probable than the flow of energy from the surrounding. This induces a time-dependent signal in the coil, which is now set in the detection mode. The signal will be either sine or cosine modulated at the precession frequency, and hence the Larmor frequency can easily be calculated by the Fourier transform which will transform the intensity as a function of time to intensity as a function of frequency, which is known as a spectrum. Since it is known where different types of protons, i.e. amide protons, alpha-protons and methyl protons etc, are located in a spectrum, the different protons can be identified.

2.2 How can Membrane Proteins be Studied by NMR?

A biological membrane is by far too large to study by high-resolution solution NMR, hence membrane mimetic systems are needed. In NMR studies membrane mimetic systems consisting of phospholipids and detergents, which can be mixed to create different membrane-like structures, i.e. micelles (Section 2.2.1.) or bicelles (Section 2.2.2.), are frequently utilized. A biological membrane is described as bulk lipids, due to the lipids ability to rotate around their vertical axis and their fast lateral diffusion. However, biological membranes contain hundreds of different lipids, which are varied to preserve membrane fluidity, and are not evenly distributed due to for example lipid raft formation. Luckily, lipid-peptide interactions are often not highly specific and thus membrane segments can be reconstituted in many different lipid compositions (33).

2.2.1 Dodecylphosphocholine Micelles

Dodecylphosphocholine (DPC) is a detergent often used to mimic zwitterionic membranes by forming micelles. Micelles are rough spheres created of detergents at concentrations over a certain threshold, the critical micelle concentration (CMC). When the detergent concentration exceeds the CMC concentration, the exceeding concentration of detergent molecules self-assemble into aggregates with their hydrophilic part facing the outside burying their hydrophobic tails inside, due to the hydrophobic effect. Ideally a CMC concentration of free detergents will thus remain free in the solution. The free detergents and the micelle-bound detergents are in rapid exchange with each other. The CMC for DPC is 1.0-1.5 mM (33, 34, 35). There is also a critical micelle temperature (CMT), which has to be exceeded for detergent monomers to be in exchange with detergent micelles instead of detergent crystals. In addition, micelles are characterized by an aggregation number (N), describing how many detergent molecules that assemble into a micelle on average. The aggregation number describing DPC is low, typically 50-60 (33, 36), and hence high-resolution spectra is obtainable i.e. since this corresponds to a molecular weight of 18-21 kDa. In contrast to many other micelle-forming lipids, DPC-micelles have a narrow size distribution at temperatures ranging from 10-50 °C and concentrations around 5-100 mM (33), which makes them very suitable for conditions often used in NMR measurements. Interestingly, in NMR studies of micelle-peptide aggregates, much higher detergent concentrations than expected from the CMC and aggregation number of DPC micelles are needed, e.g. in paper I a peptide-lipid ratio of 1:100 is used, since more lipids are needed to protect hydrophobic parts of the peptide from water (34, 37). Due to the strong curvature of micelles, hydrophobic peptides that thus are covered with lipids are more prone to adopt a native structure when reconstituted in micelles than peptides that interact with the exterior parts of the lipid-water interface. Membrane surface-interacting peptides can with greater success be studied utilizing phospholipid bicelles as membrane mimetics.

2.2.2 Phospholipid Bicelles

Bicelles (38, 39) are mixtures of long-chained phospholipids, for instance di-myristoyl-phosphatidyl-choline (DMPC) and di-myristoyl-phosphatidyl-glycerol (DMPG), with detergents, lysophospholipids or short-chained phospholipids, for instance di-hexanoyl-phosphatidyl-choline (DHPC) (Fig. 5) (40). They are disk-shaped bilayered micelles and hence have less curvature than ordinary micelles, providing a core region similar to a biological membrane. This makes bicelles especially suitable for studies of peptides (39, 41) interacting predominately with the lipid-water interface. The size of the bicelle is depending on the total lipid concentration as well as the ratio between long-chained lipids and short-chained lipids; this is called the q-value. A large q-value implies a greater amount of long-chained phospholipids in the mixture,

hence a greater bicelle. In solution NMR q-values of 0.2-0.5 are typically used to produce isotropically tumbling bicelles suitable for high-resolution studies of membrane-bound peptides (41). The ratio of DMPC to DMPG determines the acidity of the membrane (42). Interestingly, many proteins seem to prefer negatively charged membranes.

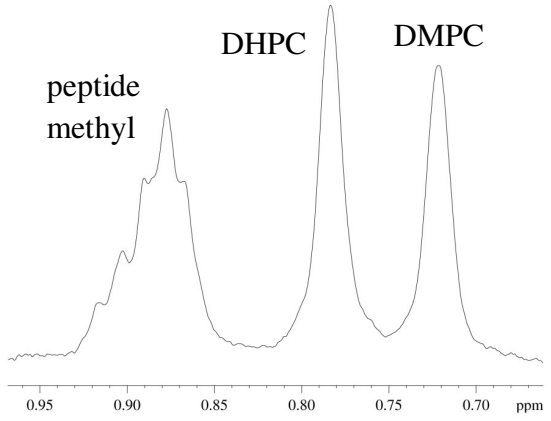

Fig. 5. The methyl proton resonances of DHPC and DMPC are often resolved from the methyl proton resonances of a peptide. Here a 1D ^{1}H spectrum of AS2p-EnvZ_{Ec} dissolved in DMPC/DHPC bicelles is seen.

2.3 Protein Structure Determination of Peptides Derived from Membrane Proteins

Structure determination of membrane-bound peptides follows the same strategies as structure determination of soluble proteins (31). Two-dimensional ^{1}H-^{1}H experiments (43) are often sufficient for complete assignment of all proton resonances in a peptide in micelles or bicelles i.e. if not too severe proton resonance overlap occur and the spectra is not hampered by broad lipid signals. The total correlation spectroscopy (TOCSY) experiment traces out the entire J-coupling network i.e. each amino acid (44). However, sometimes it can be hard to distinguish different side-chain protons in a spin system; this is enabled by the correlation spectroscopy (COSY) experiment. A COSY spectrum provides information about which protons that are J-coupled to each other i.e. have three or less chemical bonds in between each other (45). Further, with the means of the nuclear Overhauser effect spectroscopy (NOESY) experiment, amino acids that are close in space, i.e. with a dipole-dipole interaction between them, give cross peaks (46). Initially "above diagonal" cross-peaks involving H^{N} protons are assigned, since H^{N} protons are usually most resolved and the F1-dimension suffers less from water distortions as compared to the F2-dimension. A combination of the sequential assignment strategy (31) and the main chain directed approach (MCD) (47, 48) is utilized identifying some initial spin systems in the TOCSY spectrum and subsequently identifying local NOE connectivity patterns. In this way the assignment proceeds by alternating between the two assignment methods. When the assignment is complete the secondary structure of the peptide can be investigated by the means of H^{α} secondary chemical shifts (46). The chemical shifts of the alpha protons as compared to random coil shifts are indicators of secondary structure and hence provide information of dihedral angles. Further, the NOE connectivity pattern provides information of

the local secondary structure. For instance the combination of strong H^N/H^N (i, i+1) peaks and weak H^α/H^N(i, i+1) peaks indicate α-helical structure.

To calculate a 3D structure, constrains have to be deduced from the peak intensities or integrals of assigned cross-peaks in a NOESY spectra. The magnetization transfer i.e. cross relaxation from one spin to a dipole-interacting neighbor is distance dependent and hence the intensity of the peak is distance dependent too. The 3D structure calculation is a minimization problem for a target function aiming to minimize the differences between a structure and the constraints (49). The structure is refined in several steps by for instance adding restrains and changing weights for restraints to iteratively reduce assignment ambiguity. Ultimately an ensemble of structures is calculated.

2.4. Translational Diffusion Studied by Pulse Field Gradient (PFG) NMR: a Method to Study Interaction between Peptides and Membrane

In the two-dimensional experiments previously described the Hamiltonian is switched between the evolution and the acquisition, creating two dimensions and concurrently decreasing overlap of resonances and chemical shifts. However, in diffusion experiments a second dimension related to size is introduced, providing a possibility to study interaction between peptides and membrane mimetics. To illustrate, if a peptide is associated with a bicelle, it will start to diffuse as a species of the size of a bicelle, hence the translational self-diffusion will slow down. This connection arises because the translational diffusion constant is dependent on friction factors as described by the Stoke-Einstein relationship. The hydrodynamic radius, a radius of a hard sphere that diffuses at the same rate as the studied species, can be derived from the translational diffusion constant (50). As a result, if the peptide diffuses at a rate similar to the membrane mimetic, this shows that it is associating with the membrane mimetic. The percentage of peptide interacting can be deduced by assuming a two-state model; the peptide is either free in the solution or bind to the bicelle.

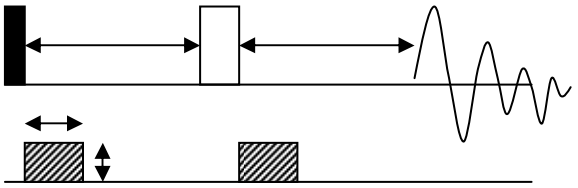

Fig. 6. The pulse field gradient spin echo (PFG-SE) experiment.Transverse magnetization, generated by a 90°-pulse, undergoes a spin echo. The spin echo will refocus the signal in the transverse plane. If a dephasing gradient precedes the refocusing pulse and a rephrasing gradient exceeds it, the Brownian motion of the peptide can be investigated, since Brownian motion will disrupt the refocusing and hence attenuate the resulting signal.

The main diffusion experiment is a pulsed field gradient spin echo (PFG-SE) experiment (Fig. 6) (51, 52, 53), where two gradients create spatial labeling of the

coherences, i.e. the precession frequency of a nuclear spin will depend on its longitudinal position. Between these gradients a delay is placed, during which translational motion can occur. A refocusing pulse is placed in the middle of the diffusion delay. Hence, if no translational motion occurs the signal will be refocused as in a standard spin echo (SE) experiment (51). If Brownian motion on the other hand does occur, the spatial labeling during the first gradient will differ from the spatial labeling during the second gradient i.e. the phase will differ. This will disrupt the refocusing of the signal, and hence attenuate it. The attenuation of the signal is described by the Stejskal-Tanner equation (52). During the experiment the gradient strength is incremented. A stronger gradient will give a more pronounced attenuation. The intensity of the signal is measured and plotted against the corresponding gradient strength according to the Stejskal-Tanner equation. The diffusion coefficient is deduced from the slope of the resulting curve.

3. Peptide and Lipid Interactions Investigated by Absorption and Emission Spectroscopy

Electronic transitions occur due to absorption or emission of light in the ultra violet (UV) to near-infrared (IR) part of the electronic spectra. This is what makes objects visible and give them their colors. However, interaction with electromagnetic radiation of this frequency range provides other information too, for instance information about the secondary structure of the chromophore (Section 3.2) and information about the chromophores immediate environment (Section 3.3).

3.1 How can Membrane Proteins be Studied by Far-UV Electronic Circular Dichroism? or LUVs as Membrane Mimetics

By far-UV electronic circular dichroism peptides can be studied under similar conditions as in NMR, hence micelles (Section 2.2.1.) and phospholipid bicelles (Section 2.2.2.) can be used as membrane mimetics. Further, large unilamellar vesicles (LUVs) can be used at low concentrations, thereby minimizing the light scattering contribution to the spectra (54). Vesicles consist of phospholipids, commonly palmitoyl-oleoyl-phosphatidylcholine (POPC) and palmitoyl-oleoyl-phosphatidyl-glycerol (POPG). Vesicles that make up a single bilayer separating the internal solution from the external solution are called unilamellar. Unilamellar vesicles have different sizes depending on how they are prepared. LUVs are usually made with a 100 nm diameter (55).

3.2 Far-UV Electronic Circular Dichroism: A Method to Study Secondary Structures of Peptides in Different Conditions

The secondary structure of peptides in different environments can be investigated by circular dichroism (CD) spectroscopy (56). Hence, CD can be used to compare the effect of different membrane mimetics on peptides, whereas similar spectra imply similar structure (Fig. 7), and for studying structure induction by membrane mimetics (Fig 8). CD refers to the difference in uptake of right-handed circularly polarized light as compared to left-handed circularly polarized light and is thus a method based on the phenomenon of chirality (57).

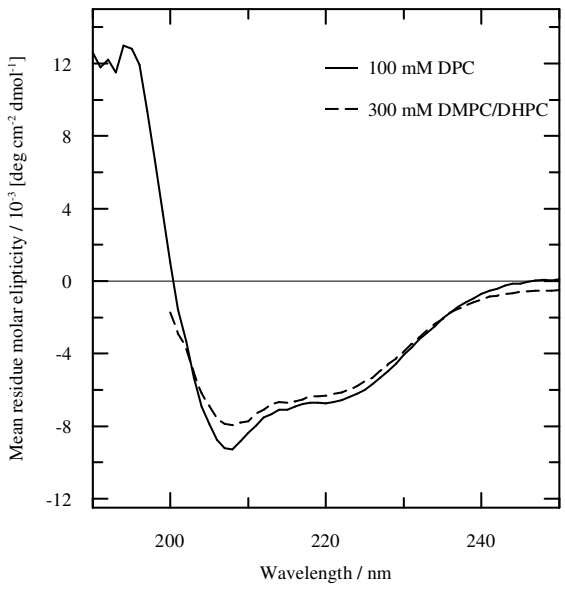

Fig. 7. Circular dichroism as a method to study secondary structure in different model membranes. Matching of a CD-spectrum of a peptide in different membrane mimetics strongly suggest that the peptide adopt similar structures in the different conditions. Here, the HsapBK K^+ Channel Voltage-Sensor Paddle Sequence is seen in DPC micelles and DMPC/DHPC bicelles, respectively.

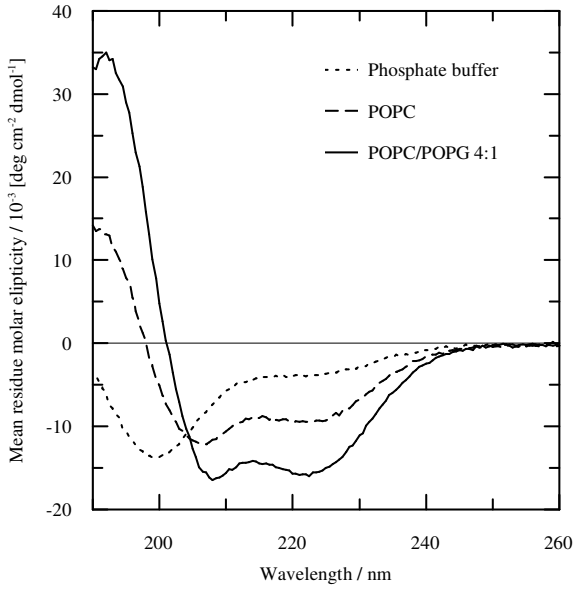

Fig. 8. Circular dichroism as a method to study induction of secondary structure. AS1p-Tar_{Ec} in phosphate buffer, POPC and POPC/POPG 4:1, respectively. In POPC this peptide becomes α-helical and even more so in POPC/POPG 4:1.

Chiral molecules are each others non identical mirror images. A property of chiral or optically active molecules is that they react differently with other chiral molecules. For instance your hands are each others non identical mirror images. Putting on a left-hand glove on the right hand will indeed give a different result than putting on a left-hand glove on the left hand, since the gloves are each others non identical mirror images too. Electromagnetic light can be made chiral and thus reacts differently with chiral chromophores in the sample.

In the far-UV spectral region (190-250 nm) the peptide bonds are the main chiral chromophores together with the aromatic sidechains, which under some circumstances contribute in this region (58). The chirality of the peptide bond arises when it is placed in a regular asymmetrically folded environment. The energy absorbed by the peptide is highly dependent on the phi and psi angles, which will thus give information about the secondary structure.

For quantitative estimation of secondary structure content, methods assuming that the experimental spectrum can be described as a linear combination of characteristic spectra of individual secondary structure components i.e. α-helix, β-sheet etc. using reference sets of proteins with known structure are used (Fig. 9) (59, 60, 61). However, special care must be taken

when studying membrane interacting peptides, since most reference data are derived from soluble globular proteins.

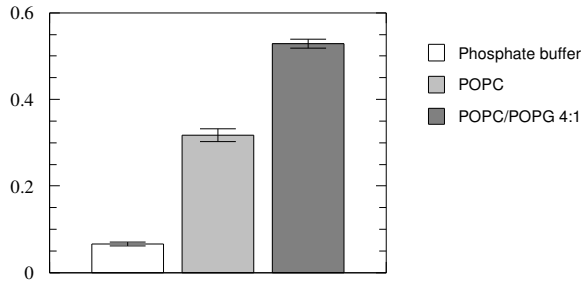

Fig. 9. The fraction of α-helix in AS1p-Tar_{Ec} in phosphate buffer, POPC and POPC/POPG 4:1, respectively, as determined by CD. Clearly, a helical induction upon addition of neutral LUVs is seen, and even more so upon addition of 20% negatively charged LUVs.

3.3 Intrinsic Tryptophan Fluorescence, or Blue-shift as an Indicator of Interaction between Peptides and Membrane

The membrane interaction of peptides containing a tryptophan can easily be studied by fluorescence spectroscopy, since tryptophan, i.e. the indole group of tryptophan, is an intrinsic fluorophore (62, 63). Fluorescence occurs when an electronically excited fluorophore returns to its ground state by emitting radiation. Fluorescence of the amino acid tryptophan is highly dependent upon the polarity of the adjacent environment. Moving a tryptophan from a polar environment to an apolar environment, i.e. from the water-lipid interface towards the hydrocarbon core of a membrane, thus results in a blue-shifted emission.

4. Interaction of HsapBK(233-260) and the HAMP-domains with Membrane Mimetics

4.1. How HsapBK(233-260) Interact with DPC Micelles

Peptide-lipid interactions are of major importance in voltage-gating of ion channels. Crystal structures of several K_v channels have been published (15, 64, 65, 66). However, a structure of the *Homo sapiens* BK channel has not yet been presented. Thus, we wanted to solve the NMR solution structure of the HsapBK(233-260) peptide corresponding to the paddle motif of HsapBK, to be able to draw important conclusions about the differences and similarities in voltage-gating among BK channels and other K_v channels.

As shown by CD spectroscopy in figure 1 in paper I, HsapBK(233-260) adopts the same structure in DPC micelles as in phospholipid bicelles. However, the presence of one hydrocarbon tail instead of two promotes micelle formation as opposed to bicelle formation. The headgroup in DPC is the same as in phosphatidylcholine, thus providing the opportunity for interaction between lipid phosphate regions and snorkeling polar amino acids (67, 68, 69). Nevertheless, HsapBK(233-260) is assumed to interact predominantly with the hydrocarbon region of the bilayer, since it is not soluble in phosphate buffer. Clearly, the CD spectra show that for HsapBK(233-260) a DPC micelle provides a sufficient hydrocarbon volume to reconstitute this peptide without adding extra strain due to the stronger curvature of the micelle as compared to the bicelle.

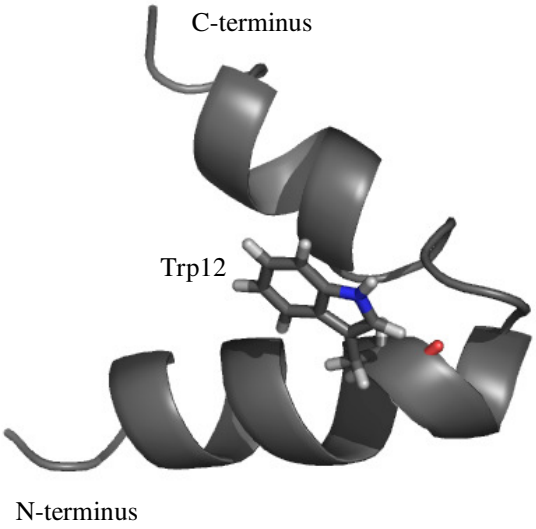

Fig. 10. Location of Trp12 in the solution structure of HsapBK(233-260) in DPC micelles. Trp12 participates in two of the six unambiguous long-range NOEs defining the interface between S3b and S4.

The blue-shift of the emission maximum of the intrinsic tryptophan fluorescence of Trp12 in HsapBK(233-260) as compared to a solvent-exposed Trp residue, clearly shows that this residue experience an environment less polar than aqueous media. A blue-shift of the same order has been shown for melittin in DPC micelles (33) and in native and artificial phospholipid membranes (70, 71), respectively, where melittin is assumed to interact with the lipid-water interface. Trp

residues are in fact over-represented near the ends of TM helices (72, 73), where they are believed to anchor proteins by interaction with the headgroup regions of lipids (67, 74, 75). To accommodate this interfacial location, both hydrogen-bond ability and aromaticity is required (72). In a Trp the hydrogen-bond ability is accommodated by the amide group, which provides a dipole moment and can act as a hydrogen bond donor. The hydrophobic ring structure provides the aromaticity. Notably, in phospholipid bicelles tryptophan residues are generally located near the carbonyl region of the phospholipid, which is not present in DPC. However, if this affects the orientation of the tryptophan, the effect is not severe enough to be seen in the CD spectra.

In the solution structure ensemble solved in paper I, Trp12 is indeed located in the bend of the helix-turn-helix motif, reaching out towards the surrounding (Fig. 10). Further, Trp12 is predicted to start the S4 domain of BK channels by multiple sequence alignment of several different voltage sensors (15). Trp has been suggested to orient transmembrane helices with respect to one another in multi-spanning membrane proteins (67). Indeed, this is seen in the solution structure of HsapBK(233-260), since Trp12 participates in two of the six unambiguous long-range NOEs defining the orientation between S3b and S4. Interestingly, this tryptophan is not found at this position in most other K_v channels i.e. in K_vAP or K_v2.1 as shown in figure 6 in paper I.

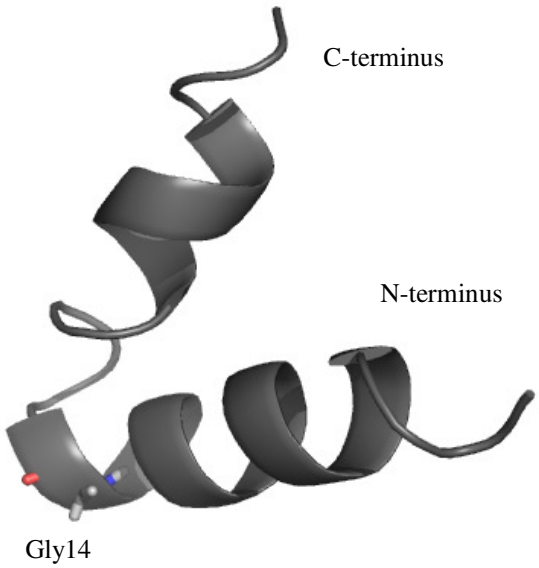

Fig. 11. The position of glycine 14 in the solution structure of HsapBK(233-260). Glycines often have structural roles in membrane proteins.

Gly14 is located close to the turn of the helix-turn-helix motif (Fig. 11). Interestingly, glycines are thought to have structural roles in transmembrane proteins, allowing helix packing, and do not disrupt α-helices to the same extent as in soluble proteins. The K_vAP channel has a glycine in the corresponding position. However, K_vAP also features two other glycines. One located within the S3b segment and one in the loop connecting S3b and S4.

PFG NMR experiments revealed that HsapBK(233-260) diffuses at a rate close to the diffusion rate of a micelle, implying similar size, and thus suggest that they interconnect. The hydrophobic character of HsapBK(233-260) and the fact that it is not readily soluble in phosphate buffer strongly suggest that this peptide is buried in the micelle. In other words, this would imply

that the association of the peptide and the micelle is predominately driven by nonpolar contributions to the association free energy. The hydrodynamic radii for DPC micelles as compared to the HsapBK(233-260)-micelle complex, as deduced from diffusion coefficients, indicates a 25% volume increase when adding HsapBK(233-269) to the micelles. The HsapBK(233-260) peptide cannot account for this increase in volume on its own, which suggests that more lipids are added to the micelle, to bury hydrophobic parts of the peptide. On the contrary, peptides that locate close to the membrane surface have been shown to displace detergents leading to a similar size of micelles and peptide-micelle complexes. Phospholipid bicelles might provide a better option for surface-associated peptides, by providing a surface more alike the surface of biological membranes.

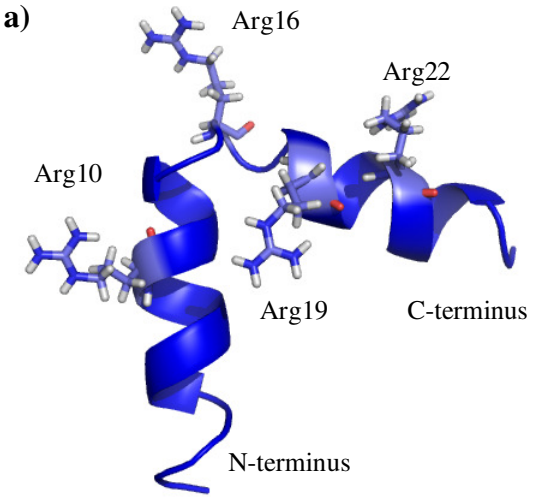

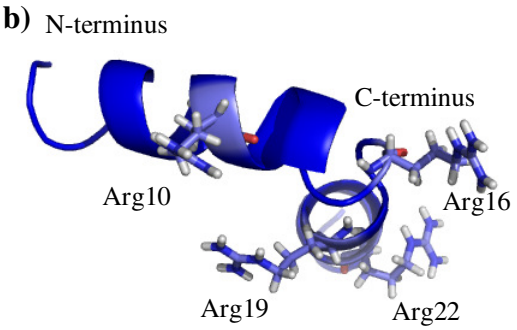

Fig. 12. The position of the four arginines in the solution structure of HsapBK(233-260). The side-chains of the four Arg residues are depicted. a) shows a front view while b) shows a view down along the C-terminal S4 helix, indicating that the Arg residues are all on the outside of the structure.

In the solution structure of HsapBK(233-260) in DPC micelles it is clearly seen that all polar residues i.e. Arg, Pro, Glu, Gln and Asn are pointing out from the helix-turn-helix motif. Notably, the overlap in the spectra is too severe to strictly define side-chain orientation in this solution structure ensemble. However, this indicates that the peptide is positioned inside of the micelle and that the polar amino acids are reaching out for interactions with the headgroups, even though more experiments would have to be acquired to affirm this, for instance ^{13}C-relaxation experiments. However, the occurrence of interactions between the peptide and polar headgroups suggest that the peptide is located close to the lipid-water interface.

The arginines are of special interest, since they constitute the gating charges that are believed to move to open the channel pore (Fig 12). Interestingly, the high

arginine content of CPPs is related to their membrane translocation properties (76, 77), indicating that arginines are important for movement of peptides within membranes. The guadinium groups bind soft anions strongly e.g. phosphate groups, both through charge pairing by their delocalized positive charge i.e. below pH 12.5, and through hydrogen bonding. In addition, arginines can be either hydrophilic or lipophilic depending on nearby counter ions (78, 79). The membrane interaction of arginines could thus readily be modulated.

In the *Shaker* K^+ channels it has been shown that the S3b net charge does not modify the gating charge (80), as proposed by the paddle model. This seems to be a general feature of channels featuring a long S3-S4 linker (80). On the other hand, electrophysiological studies show that in BK channels gating charges are also contributed from S3 and S2 (81). This indicates that the voltage-gating mechanisms applied by different channels, may indeed be more diverse than previously believed.

4.2 Helical Induction as a Probe for Signal Transduction Mechanism of HAMP-domains

The HAMP domains are often found just inside of the cell membrane. Nevertheless, present studies of HAMP domain structure and function do not investigate how the cell membrane influences the character of these domains. Hence, we wanted to study the membrane affect on AS1 and AS2 of the HAMP domains of four well characterized sensor proteins; Af1503, $EnvZ_{Ec}$, $NarX_{Ec}$ and Tar_{Ec}.

In paper II it is shown by PFG NMR that AS1-$NarX_{Ec}$, AS1-Tar_{Ec} and AS2-$Af1503_{Ec}$ bind strongly to both neutral and 20% negatively charged phospholipid bicelles, i.e. approximately 100% of the peptide is bound. At pH 7.2 all of these peptides are positively charged, which suggests that electrostatic interactions contribute to the free energy of association. Association with the phosphates in the headgroups of the phospholipids seems plausible, since the addition of DMPG is not needed for strong binding. Interestingly, AS2p-$EnvZ_{Ec}$ is positively charged too, but does not bind as strong, implying that the electrostatic interaction is not sufficient for strong membrane association.

Further, AS1-$NarX_{Ec}$ and AS1-Tar_{Ec} contain 61% and 67% nonpolar residues, respectively, whereas AS2-$Af1503_{Ec}$ and AS2p-$EnvZ_{Ec}$ comprise only 39% and 44% nonpolar residues, respectively. Together with AS2-$NarX_{Ec}$, AS1- $NarX_{Ec}$ and AS1-Tar_{Ec} have the highest average hydrophobicity. This indicates that hydrophobic interactions also are important for membrane interaction. For this reason, the peptide seems to partially penetrate the lipid bilayer interacting with both headgroups and the hydrocarbon region. Notably, AS2-$NarX_{Ec}$ does not bind phospholipid bicelles as strong; therefore hydrophobicity is not sufficient for strong membrane interaction either. The positive charge in the peptide is probably needed for adsorption to the negatively charged phosphate groups in the lipid bilayer, whilst

the hydrophobicity enables further penetration into the lipid-water interface.

As seen by CD in paper II, membrane based α-helical induction, upon addition of zwitterionic or 20% negatively charged LUVs, is only seen in AS1-NarX$_{Ec}$ and AS1-Tar$_{Ec}$. The penetration into the lipid-water interface is probably driven by the hydrophobic effect and the stabilization of hydrogen bonding along the backbone. AS2p-Af1503 is unique among these peptides, since it interacts strongly with phospholipid bicelles, but remains structured to the same extent under all experimental conditions. There is also an interesting difference between AS1-NarX$_{Ec}$ and AS1-Tar$_{Ec}$; while AS1-Tar$_{Ec}$ adopts α-helical structure in both zwitterionic and 20% negatively charged LUVs, AS1-NarX$_{Ec}$ only adopts α-helical structure in 20% negatively charged LUVs. The primary structure of AS1-NarX$_{Ec}$ contains three Arg-residues as compared to two in AS1-Tar$_{Ec}$. The neutralization of these arginines by negative charge at the surface of the bicelle, seems to be necessary for establishing regular secondary structure of AS1-NarX$_{Ec}$. This has also been suggested for other membrane-interacting peptides (82). Surprisingly, the negative charge is not needed for strong interaction as seen by PFG NMR. This might be due to differences between the two membrane mimetics, or perhaps the positive charge and hydrophobicity of this peptide is enough for interaction with the lipid-water interface, without structural induction. When adding negative charge to the LUVs, on the other hand, α-helical structure is induced. Notably, the inside of the *E.coli* membrane is indeed negatively charged at rest.

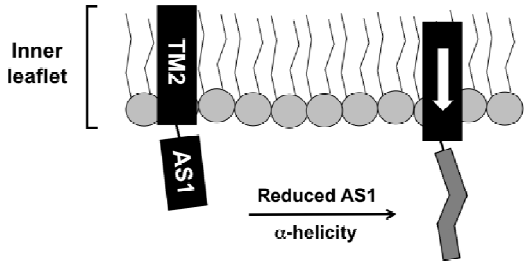

Fig. 13 Piston-type displacements of TM2 in sensor proteins may reduce membrane-induced helicity within AS1 and thereby act as a switch in the signal transduction. Based on our results in paper II the HAMP-domains from NarX$_{Ec}$ and Tar$_{Ec}$ are proposed to transfer signals from the membrane toward the catalytic core by conformational changes induced by changes in membrane-interaction, brought about by conformational changes in the transmembrane helices.

Based on our study in paper II the HAMP domains can be divided into two groups considering their membrane interaction features. The group consisting of NarX$_{Ec}$ and Tar$_{Ec}$ is distinguished by showing helical induction in AS1 upon addition of negatively charged LUVs. Further, the AS1 peptides of NarX$_{Ec}$ and Tar$_{Ec}$ interact strongly with bicelles as showed by diffusion NMR. The group consisting of Af1503 and EnvZ$_{Ec}$, on the contrary, does not show any helical induction in AS1 upon addition of LUVs, and their AS1 segments do not interact as strongly with bicelles. Interestingly, NarX$_{Ec}$ and Tar$_{Ec}$ are suggested to share a common mechanism of transmembrane signaling (83)

involving a periplasmic four-helix bundle. Piston-type displacement of transmembrane helix 2 (TM2) in this four-helix bundle could alter the position of AS1 and hence influence its propensity for α-helix formation (Fig. 13). We suggest that a correlation exists between helical induction in AS1 and this mechanism of transmembrane communication. The HAMP-domains of Af1503 and $EnvZ_{Ec}$, on the contrary, are suggested to function by a membrane-independent mechanism.

4.3 Membrane Interaction of Peptides: General Features

There are different types of membrane interacting proteins. Some interact predominately with the surface of the biological membrane i.e. the exterior and more polar part of the lipid-water interface. For these proteins membrane-interaction is established by electrostatic interactions. Other proteins are buried inside of the hydrophobic core, and hydrophobic interaction dominates the association free energy. However, many membrane interacting proteins localize deep within the lipid-water interface penetrating the hydrophobic core, thus both electrostatic and hydrophobic interactions are important. For HsapBK(233-260), AS1-$NarX_{Ec}$ and AS1-Tar_{Ec} both charge and hydrophobicity seems to be crucial for membrane interaction.

Interestingly, all of these peptides contain a Pro residue N-terminally. For K_v channels this proline is conserved among different channel types. Further, this proline is also conserved among the four different AS1 segments studied in paper II. Prolines have been suggested to create hinges in structures, which enable conformational transitions. For AS1-$NarX_{Ec}$ and AS1-Tar_{Ec} such a hinge could transform the movement of TM2 into a movement of AS1 away from the membrane, which affects the secondary structure of this segment. Likewise, if S3b moves as described in the paddle model, a hinge between S3a and S3b, could indeed provide the flexibility for S3b movement.

Movement of peptides within the membrane seems to be strongly associated with the occurrence of arginines in their primary structure. Many of the AS1- and AS2-segments of the studied HAMP domains, also contains some arginines. The ability of a peptide to move within a membrane is dependent on the ability of modulation of electrostatic interaction as well as hydrophobicity and hydrogen bonding. These properties can indeed be varied for an arginine in a lipid-water interface.

5. ACKNOWLEDGEMENTS

This licentiate thesis summarizes my work during my first three years in the group of Dr. Lena Mäler in the Department of Biophysics at Stockholm University. During this time I have had the privilege of working with many creative and inspiring co-workers, whom I would like to acknowledge here.

First, I would like to show my gratitude to my supervisor Dr. Lena Mäler for providing many interesting research projects and for being available on an almost daily-basis! I would also like to thank Lena for encouraging cooperation within her group, and through this creating a positive learning environment. Further, I would like to acknowledge present and past members of the Mäler NMR group. It is my pleasure to thank Drs. Jesper Lind and Henrik Biverståhl for their invaluable support and guidance through my first years as a PhD student, and during my first visit to US. Especially, I would like to thank Jesper for many interesting scientific discussions and for inspiring cooperation on Paper I. Moreover, I am grateful for my brief but insightful work with Dr. Andrea Bodor, and I sincerely hope that there will be more opportunities in the future. I am very grateful for the pleasant times I have had with Scarlett Spryngiel, especially during our time together at the Swedish NMR Center in Gothenburg. Finally, I give my deepest appreciation to our newest members Ye Weihua and Johannes Björnerås, who always puts a smile on my face, and have already contributed a lot to the scientific atmosphere of the Mäler group.

Second, I would like to thank my second supervisor Prof. Astrid Gräslund for being a role-model within the field of biophysics. In addition, I would like to acknowledge members of the Gräslund group. Particularly, I would like to show my gratitude to Anna Wahlström for being my speaking-partner before we ever dared to have scientific discussions with anyone else. Further, I would like to acknowledge Dr. Elsa Bárány-Wallje for never giving up on finding the lock-frequency at the old 600 MHz spectrometer, and for finding even the most annoying problems interesting. Moreover, I am indebted to Tariq Massad for inspiring discussions, which contributed a lot to my time as a PhD student. I would also like to thank Fatemeh Madani for teaching me how to prepare LUVs and how to use them in CD, and for her support. I would also like to acknowledge Dr. Alex Perálvarez-Marín for teaching me about the lag-phase and the log-phase in paper publishing during a PhD, which is a comforting thought at times. I am grateful for the intressting discussions and walks with Axel Abelein. I would also like to acknowledge Dr. Evangelos Papadopoulos for teaching me how to use SPARKY and thereby contributing to Paper I. Additionally, I would like to thank: Drs. Peter Damberg and Sebastian Wärmländer for all inspiring discussions; Dr. Jüri Jarvet for helping with shimming, nitrogen-sticks and tuning and matching at the old Varian Inova spectrometer and finally Dr. Jens Danielsson for good advices regarding translational diffusion measurements.

It is my pleasure to acknowledge Torbjörn Astlind for invaluable technical support, and for encouraging even the most daring projects, i.e. the venturesome NMR spectrometer building project, and even more foolhardy, the keeping pot-plants alive project. I would also like to thank

Haidi Astlind and Britt-Marie Olsson for providing administrative support, making my life so much easier.

This thesis would not have been possible without the inspiring cooperation with Prof. Gunnar von Heijne and Dr. Roger Draheim on Paper II. It is always great fun to work with Roger Draheim. I especially thank Roger for introducing me to the intriguing field of HAMP-domains. Further, I owe my greatest gratitude to the PhD Coucil: Charlotta Andersson, Tiago Selao, Emelie Svahn, Linnea Hedin, Karin Skaar, Aron Hennerdal and Pär Bjelkmar. I think we have come a long way during my years at DBB, and I hope we will inspire even more PhD students to join us.

Last but not least I thank my family and friends. Martina Unnerståle for saying things like "One day Boron will be removed from the periodic table and you will have to live with that, without questioning" that put things in perspective. My special thanks go to Linda and Mira Salmén, whom I nowadays regard as my family. I would also like to acknowledge Per and Ann-Britt Unnerståle for supporting me and keeping me alive at times. I thank Jens Bergensten and Daniel Niska for always being up for a weekday-adventure. I owe my deepest gratitude to Dr. Kristina Westerlund for being a wonderful friend. Finally, I want to thank my friends from the Stockholm Graduate School of Molecular Life Science; Masako Harada, Annelie Strålfors, Jeanette Grundström, Karin Sundström and Eva Daskalaki. Without you, this rollercoaster-ride would not have been half as interesting or fun!

Sincerely yours

6. REFERENCES

1. Hodgkin, A. L., and Huxley, A. F. (1990) A Quantitative Description of Membrane Current and its Application to Conduction and Excitation in Nerve. *Bull. Math. Biol. 52*, 25-71.

2. Noda, M., Shimizu, S., Tanabe, T., Takai, T., Kayano, T., Ikeda, T., Takahashi, H., Nakayama, H., Kanaoka, Y., and Minamino, N. (1984) Primary Structure of Electrophorus Electricus Sodium Channel Deduced from cDNA Sequence. *Nature. 312*, 121-127.

3. Bezanilla, F. (2000) The Voltage Sensor in Voltage-Dependent Ion Channels. *Physiol. Rev. 80*, 555-592.

4. Bezanilla, F. (2002) Voltage Sensor Movements. *J. Gen. Physiol. 120*, 465-473.

5. Armstrong, C. M., and Bezanilla, F. (1974) Charge Movement Associated with the Opening and Closing of the Activation Gates of the Na Channels. *J. Gen. Physiol. 63*, 533-552.

6. Miller, C. (2000) An Overview of the Potassium Channel Family. *Genome Biol. 1*, 0004.1-0004.5.

7. Jan L.Y., J. Y. N. (1989) Voltage-Sensitive Ion Channels. *Cell. 56*, 13-25.

8. Jan, L. Y., and Jan, Y. N. (1997) Cloned Potassium Channels from Eukaryotes and Prokaryotes. *Annu. Rev. Neurosci. 20*, 91-123.

9. Pallotta, B. S. (1985) N-Bromoacetamide Removes a Calcium-Dependent Component of Channel Opening from Calcium-Activated Potassium Channels in Rat Skeletal Muscle. *J. Gen. Physiol. 86*, 601-611.

10. Marty, A. (1981) Ca-Dependent K^+ Channels with Large Unitary Conductance in Chromaffin Cell Membranes. *Nature. 291*, 497-500.

11. Wallner M., Meera P., Toro L. (1996) Determinant for Beta-Subunit Regulation in High-Conductance Voltage-Activated and Ca^{2+}-Sensitive K^+ Channels: An Additional Transmembrane Region at the N Terminus. *Proc. Natl. Acad. Sci. U. S. A. 93*, 14922-14927.

12. Meera, P., Wallner, M., Song, M., and Toro, L. (1997) Large Conductance Voltage-and Calcium-Dependent K^+ Channel, a Distinct Member of Voltage-Dependent Ion Channels with Seven N-Terminal Transmembrane Segments (S0-S6), an Extracellular N Terminus, and an Intracellular (S9-S10) C Terminus. *Proc. Natl. Acad. Sci. U.S.A. 94*, 14066-14071.

13. Jiang, Y., Pico, A., Cadene, M., Chait, B. T., and MacKinnon, R. (2001) Structure of the RCK Domain from the E. Coli K^+ Channel and Demonstration of its Presence in the Human BK Channel. *Neuron. 29*, 593-601.

14. Wei, A., Solaro, C., Lingle, C., and Salkoff, L. (1994) Calcium Sensitivity of BK-Type KCa Channels Determined by a Separable Domain. *Neuron. 13*, 671-681.

15. Jiang, Y., Lee, A., Chen, J., Ruta, V., Cadene, M., Chait, B. T., and MacKinnon, R. (2003) X-Ray Structure of a Voltage-Dependent K^+ Channel. *Nature. 423*, 33-41.

16. Nixon, B. T., Ronson, C. W., and Ausubel, F. M. (1986) Two-Component Regulatory Systems Responsive to Environmental Stimuli Share Strongly Conserved Domains with the Nitrogen Assimilation Regulatory Genes ntrB and ntrC. *Proc Natl Acad Sci U S A. 83*, 7850-7854.

17. Stock, J. B., Ninfa, A. J., and Stock, A. M. (1989) Protein Phosphorylation and Regulation of Adaptive Responses in Bacteria. *Microbiol. and Mol. Biol. Rev. 53*, 450-490.

18. Hoch, J. A. (2000) Two-Component and Phosphorelay Signal Transduction. *Curr. Opin. Microbiol. 3*, 165-170.

19. Szurmant, H., White, R. A., and Hoch, J. A. (2007) Sensor Complexes Regulating Two-Component Signal Transduction. *Curr. Opin. Struct. Biol. 17*, 706-715.

20. Williams, S. B., and Stewart, V. (1999) Functional Similarities among Two-Component Sensors and Methyl-Accepting Chemotaxis Proteins Suggest a Role for Linker Region Amphipathic Helices in Transmembrane Signal Transduction. *Mol. Microbiol. 33*, 1093-1102.

21. Kalman, L. V., and Gunsalus, R. P. (1990) Nitrate-and Molybdenum-Independent Signal Transduction Mutations in narX that Alter Regulation of Anaerobic Respiratory Genes in Escherichia Coli. *J. Bacteriol. 172*, 7049-7056.

22. Forst, S., Comeau, D., Norioka, S., and Inouye, M. (1987) Localization and Membrane Topology of EnvZ, a Protein Involved in Osmoregulation of OmpF and OmpC in Escherichia Coli. *J. Biol. Chem. 262*, 16433-16438.

23. Liljeström, P. (1986) The EnvZ Protein of Salmonella Typhimurium LT-2 and Escherichia Coli K-12 is Located in the Cytoplasmic Membrane. *FEMS Microbiol. Lett. 36*, 145-150.

24. Hall, M. N., and Silhavy, T. J. (1981) The ompB Locus and the Regulation of the Major Outer Membrane Porin Proteins of Escherichia Coli K12. *J. Mol. Biol. 146*, 23-43.

25. Blair, D. F. (1995) How Bacteria Sense and Swim. *Annu. Rev. Microbiol. 49*, 489-520.

26. Falke, J. J., Bass, R. B., Butler, S. L., Chervitz, S. A., and Danielson, M. A. (1997) The Two-Component Signaling Pathway of Bacterial Chemotaxis: A Molecular View of Signal Transduction by Receptors, Kinases, and Adaptation Enzymes. *Annu. Rev. Cell Dev. Biol. 13*, 457-512.

27. Milligan, D. L., and Koshland Jr, D. E. (1988) Site-Directed Cross-Linking. *J. Biol. Chem. 263*, 6268–6275.

28. Aravind, L., and Ponting, C. P. (1999) The Cytoplasmic Helical Linker Domain of Receptor Histidine Kinase and Methyl-Accepting Proteins is Common to Many Prokaryotic Signalling Proteins. *FEMS Microbiol. Lett. 176*, 111-116.

29. Butler, S. L., and Falke, J. J. (1998) Cysteine and Disulfide Scanning Reveals Two Amphiphilic Helices in the Linker Region of the Aspartate Chemoreceptor†. *Biochemistry (N. Y.). 37*, 10746-10756.

30. Hulko, M., Berndt, F., Gruber, M., Linder, J. U., Truffault, V., Schultz, A., Martin, J., Schultz, J. E., Lupas, A. N., and Coles, M. (2006) The HAMP Domain Structure Implies Helix Rotation in Transmembrane Signaling. *Cell. 126*, 929-940.

31. Wuthrich, K. (1986) *NMR of Proteins and Nucleic Acids.* John Wiley & Sonc, Inc., US.

32. Bloch, F., Hansen, W. W., and Packard, M. (1946) Nuclear Induction. *Phys. Rev. 70*, 460-474.

33. Lauterwein, J., Bosch, C., Brown, L. R., and Wuthrich, K. (1979) Physicochemical Studies of the Protein-Lipid Interactions in Melittin-Containing Micelles. *Biochim. Biophys. Acta. 556*, 244-264.

34. Kallick, D. A., Tessmer, M. R., Watts, C. R., and Li, C. Y. (1995) The use of Dodecylphosphocholine Micelles in Solution NMR. *J. Magn. Reson. Ser. B. 109*, 60-65.

35. le Maire, M., Champeil, P., and Møller, J. V. (2000) Interaction of Membrane Proteins and Lipids with Solubilizing Detergents. *Biochim. Biophys. Acta. 1508*, 86-111.

36. Brown, L. R., Bösch, C., and Wüthrich, K. (1981) Location and Orientation Relative to the Micelle Surface for Glucagon in Mixed Micelles with Dodecylphosphocholine EPR and NMR Studies. *Biochim. Biophys. Acta. 642*, 296-312.

37. Beswick, V., Guerois, R., Cordier-Ochsenbein, F., Coïc, Y. M., Huynh-Dinh, T., Tostain, J., Noël, J. P., Sanson, A., and Neumann, J. M. (1998) Dodecylphosphocholine Micelles as a Membrane-Like Environment: New Results from NMR Relaxation and Paramagnetic Relaxation Enhancement Analysis. *Eur. Biophys. J. 28*, 48-58.

38. Ram, P., and Prestegard, J. H. (1988) Magnetic Field Induced Ordering of Bile salt/phospholipid Micelles: New Media for NMR Structural Investigations. *Biochim. Biophys. Acta. 940*, 289-294.

39. Vold, R. R., and Prosser, R. S. (1996) Magnetically Oriented Phospholipid Bilayerd Micelles for Structural Studies of Polypeptides. does the Ideal Bicelle Exist? *J. Magn. Reson. 113*, 267-271.

40. Sanders, C. R., and Schwonek, J. P. (1992) Characterization of Magnetically Orientable Bilayers in Mixtures of Dihexanoylphosphatidylcholine and Dimyristoylphosphatidylcholine by Solid-State NMR. *Biochemistry (N. Y.). 31*, 8898-8905.

41. Vold, R. R., Prosser, R. S., and Deese, A. J. (1997) Isotropic Solutions of Phospholipid Bicelles: A New Membrane Mimetic for High-Resolution NMR Studies of Polypeptides. *J. Biomol. NMR. 9*, 329-335.

42. Struppe, J., Whiles, J. A., and Vold, R. R. (2000) Acidic Phospholipid Bicelles: A Versatile Model Membrane System. *Biophys. J. 78*, 281-289.

43. Ernst, R. R., Bodenhausen, G., and Wokaun, A. (1990) *Principles of Nuclear Magnetic Resonance in One and Two Dimensions.* Oxford University Press, USA, .

44. Braunschweiler, L., and Ernst, R. R. (1983) Coherence Transfer by Isotropic Mixing: Application to Proton Correlation Spectroscopy. *Journal of Magnetic Resonance (1969). 53*, 521-528.

45. Aue, W. P., Bartholdi, E., and Ernst, R. R. (1976) Two-dimensional Spectroscopy. Application to Nuclear Magnetic Resonance. *J. Chem. Phys. 64*, 2229-2246.

46. Wishart, D. S., Sykes, B. D., and Richards, F. M. (1992) The Chemical Shift Index: A Fast and Simple Method for the Assignment of Protein Secondary Structure through NMR Spectroscopy. *Biochemistry (N. Y.). 31*, 1647-1651.

47. Englander, S. W., and Wand, A. J. (1987) Main-Chain-Directed Strategy for the Assignment of 1H NMR Spectra of Proteins. *Biochemistry. 26*, 5953-5958.

48. Di Stefano, D. L., and Wand, A. J. (1987) Two-Dimensional 1H NMR Study of Human Ubiquitin: A Main Chain Directed Assignment and Structure Analysis. *Biochemistry. 26*, 7272-7281.

49. Güntert, P. (2004) Automated NMR Structure Calculation with CYANA. *Methods Mol. Biol. 278*, 353-378.

50. Cantor, C. R., and Schimmel, P. R. (1980) Size and Shape of Macromolecules. Biophysical Chemistry, Part II: Techniques for the Study of Biological Structure and Function, in pp 539–590, WH Freeman and Company, New York.

51. Hahn, E. L. (1950) Spin Echoes. *Phys. Rev. 80*, 580-594.

52. Stejskal, E. O., and Tanner, J. E. (1965) Spin Diffusion Measurements: Spin Echoes in the Presence of a Time-Dependent Field Gradient. *J. Chem. Phys. 42*, 288-292.

53. Wu, D. H., Chen, A. D., and Johnson, C. S. (1995) An Improved Diffusion-Ordered Spectroscopy Experiment Incorporating Bipolar-Gradient Pulses. *J. Magn. Reson. Ser. A. 115*, 260-264.

54. Magzoub, M., Kilk, K., Eriksson, L. E., Langel, Ü., and Gräslund, A. (2001) Interaction and Structure Induction of Cell-Penetrating Peptides in the Presence of Phospholipid Vesicles. *Biochim. Biophys. Acta. 1512*, 77-89.

55. Hope, M. J., Bally, M. B., Webb, G., and Cullis, P. R. (1985) Production of Large Unilamellar Vesicles by a Rapid Extrusion Procedure. Characterization of Size Distribution, Trapped Volume and Ability to Maintain a Membrane Potential. *Biochim. Biophys. Acta. 812*, 55-65.

56. Kelly, S. M., Jess, T. J., and Price, N. C. (2005) How to Study Proteins by Circular Dichroism. *Biochim. Biophys. Acta. 1751*, 119-139.

57. Rodger, A., and Nordén, B. (1997) *Circular Dichroism and Linear Dichroism.* Oxford University Press, USA, .

58. Krittanai, C., and Johnson, W. C. (1997) Correcting the Circular Dichroism Spectra of Peptides for Contributions of Absorbing Side Chains. *Anal. Biochem. 253*, 57-64.

59. Lobley, A., Whitmore, L., and Wallace, B. A. (2002) DICHROWEB: An Interactive Website for the Analysis of Protein Secondary Structure from Circular Dichroism Spectra. *Bioinformatics. 18*, 211-212.

60. Whitmore, L., and Wallace, B. A. (2004) DICHROWEB, an Online Server for Protein Secondary Structure Analyses from Circular Dichroism Spectroscopic Data. *Nucleic. Acids. Res. 32*, W668.

61. Provencher, S. W., and Gloeckner, J. (1981) Estimation of Globular Protein Secondary Structure from Circular Dichroism. *Biochemistry (N. Y.). 20*, 33-37.

62. Vivian, J. T., and Callis, P. R. (2001) Mechanisms of Tryptophan Fluorescence Shifts in Proteins. *Biophys. J. 80*, 2093-2109.

63. Lakowicz, J. R. (1999) *Principles of Fluorescence Spectroscopy.* Kluwer Academic / Plenum Publishers, U.S.A.

64. Long, S. B., Campbell, E. B., and MacKinnon, R. (2005) Crystal Structure of a Mammalian Voltage-Dependent Shaker Family K^+ Channel. *Science. 309*, 897-903.

65. Lee, S. Y., Lee, A., Chen, J., and MacKinnon, R. (2005) Structure of the KvAP Voltage-Dependent K^+ Channel and its Dependence on the Lipid Membrane. *Proc. Natl. Acad. Sci. U. S. A. 102*, 15441-15446.

66. Long, S. B., Tao, X., Campbell, E. B., and MacKinnon, R. (2007) Atomic Structure of a Voltage-Dependent K^+ Channel in a Lipid Membrane-Like Environment. *Nature. 450*, 376-382.

67. Killian, J. A., and von Heijne, G. (2000) How Proteins Adapt to a Membrane-Water Interface. *Trends Biochem. Sci. 25*, 429-434.

68. Segrest, J. P., De Loof, H., Dohlman, J. G., Brouillette, C. G., and Anantharamaiah, G. M. (1990) Amphipathic Helix Motif: Classes and Properties. *Proteins. 8*, 103-117.

69. de Planque, M. R. R., Kruijtzer, J. A. W., Liskamp, R. M. J., Marsh, D., Greathouse, D. V., Koeppe, R. E., de Kruijff, B., and Killian, J. A. (1999) Different Membrane Anchoring Positions of Tryptophan and Lysine in Synthetic Transmembrane α-Helical Peptides. *J. Biol. Chem. 274*, 20839-20846.

70. Mollay, C., Kreil, G., and Berger, H. (1976) Action of Phospholipases on the Cytoplasmic Membrane of Escherichia Coli. Stimulation by Melittin. *Biochim. Biophys. Acta. 426*, 317-324.

71. Dufourcq, J., and Faucon, J. F. (1977) Intrinsic Fluorescence Study of Lipid-Protein Interactions in Membrane Models. Binding of Melittin, an Amphipathic Peptide, to Phospholipid Vesicles. *Biochim. Biophys. Acta. 467*, 1-11.

72. Ulmschneider, M. B., and Sansom, M. S. P. (2001) Amino Acid Distributions in Integral Membrane Protein Structures. *Biochim. Biophys. Acta. 1512*, 1-14.

73. Beuming, T., and Weinstein, H. (2004) A Knowledge-Based Scale for the Analysis and Prediction of Buried and Exposed Faces of Transmembrane Domain Proteins. *Bioinformatics. 20*, 1431-1435.

74. Wimley, W. C., and White, S. H. (1996) Experimentally Determined Hydrophobicity Scale for Proteins at Membrane Interfaces. *Nat. Struct. Biol. 3*, 842-848.

75. Yau, W. M., Wimley, W. C., Gawrisch, K., and White, S. H. (1998) The Preference of Tryptophan for Membrane Interfaces. *Biochemistry (N. Y.). 37*, 14713-14718.

76. Vivès, E., Brodin, P., and Lebleu, B. (1997) A Truncated HIV-1 Tat Protein Basic Domain Rapidly Translocates through the Plasma Membrane and Accumulates in the Cell Nucleus. *J. Biol. Chem. 272*, 16010-16017.

77. Wender, P. A., Mitchell, D. J., Pattabiraman, K., Pelkey, E. T., Steinman, L., and Rothbard, J. B. (2000) The Design, Synthesis, and Evaluation of Molecules that Enable Or Enhance Cellular Uptake: Peptoid Molecular Transporters. *Proc. Natl. Acad. Sci. U. S. A. 97*, 13003-13008.

78. Nishihara, M., Perret, F., Takeuchi, T., Futaki, S., Lazar, A. N., Coleman, A. W., Sakai, N., and Matile, S. (2005) Arginine Magic with New Counterions Up the Sleeve. *Org. Biomol. Chem. 3*, 1659-1669.

79. Sakai, N., Futaki, S., and Matile, S. (2006) Anion Hopping of (and on) Functional Oligoarginines: From Chloroform to Cells. *Soft Matter. 2*, 636-641.

80. Gonzalez, C., Morera, F. J., Rosenmann, E., Alvarez, O., and Latorre, R. (2005) S3b Amino Acid Residues do Not Shuttle Across the Bilayer in Voltage-Dependent Shaker K^+ Channels. *Proc. Natl. Acad. Sci. U. S. A. 102*, 5020-5025.

81. Pantazis, A., Gudzenko, V., Savalli, N., Sigg, D., and Olcese, R. (2010) Operation of the Voltage Sensor of a Human Voltage- and Ca^{2+}-Aktivated K^+ channel . *Proc. Natl. Acad. Sci. U. S. A. 107*, 4459-4464.

82. Gawrisch, K., Han, K. H., Yang, J. S., Bergelson, L. D., and Ferretti, J. A. (1993) Interaction of Peptide Fragment 828-848 of the Envelope Glycoprotein of Human Immunodeficiency Virus Type I with Lipid Bilayers. *Biochemistry. 32*, 3112-3118.

83. Collins, L. A., Egan, S. M., and Stewart, V. (1992) Mutational Analysis Reveals Functional Similarity between NARX, a Nitrate Sensor in Escherichia Coli K-12, and the Methyl-Accepting Chemotaxis Proteins. *J. Bacteriol. 174*, 3667-3675.

I. Solution Structure of the HsapBK K^+ Channel Voltage-Sensor Paddle Sequence

BIOCHEMISTRY
including biophysical chemistry & molecular biology
Article

Biochemistry **2009,** *48,* 5813–5821 5813
DOI: 10.1021/bi9004599

Solution Structure of the HsapBK K^+ Channel Voltage-Sensor Paddle Sequence[†,‡]

Sofia Unnerståle, Jesper Lind, Evangelos Papadopoulos, and Lena Mäler*

Department of Biochemistry and Biophysics, Center for Biomembrane Research, The Arrhenius Laboratories for Natural Sciences, Stockholm University, SE-106 91 Stockholm, Sweden

Received March 17, 2009; Revised Manuscript Received May 19, 2009

ABSTRACT: Voltage-gated potassium channels open and close in response to changes in the membrane potential. In this study, we have determined the NMR solution structure of the putative S3b−S4 voltage-sensor paddle fragment, the part that moves to mediate voltage gating, of the HsapBK potassium channel in dodecylphosphocholine (DPC) micelles. This paper presents the first structure of the S3b−S4 fragment from a BK channel. Diffusion coefficients as determined from PFG NMR experiments showed that a well-defined complex between the peptide and DPC molecules was formed. The structure reveals a helix−turn−helix motif, which is in agreement with crystal structures of other voltage-gated potassium channels, thus indicating that it is feasible to study the isolated fragment. The paddle motifs generally contain several basic residues, implicated in the gating. The critical Arg residues in this structure all reside on the surface, which is in agreement with crystal structures of K_v channels. Similarities in the structure of the S3b−S4 fragment in BK and K_v channels as well as important differences are seen, which may be important for explaining the details in paddle movement within a bilayer.

Potassium channels were originally described as the membrane proteins that, during an action potential, open their pore and allow a flow of K^+ ions out of the neuron, to further enhance the restoration of the resting potential, brought about by spontaneous inactivation of voltage-gated sodium channels (*1*). However, now it is known that potassium channels are involved in many physiological functions and can be found in all types of organisms and cells (*2*, *3*). Potassium channels are highly conserved: they are all tetrameric membrane proteins that specifically conduct K^+ through an aqueous pore. Structurally, potassium channels can be divided into two major classes: the six-transmembrane-helix voltage-gated (K_v) and the two-transmembrane-helix inward rectifiers (K_{ir}).

K_v channels are homotetramers (*4*) in which each subunit contains six transmembrane segments, S1−S6. Crystal structures of K_v and of a Shaker family K^+ channel have revealed that the K_v channels are composed of two structural units, the pore domain with the selectivity filter (segments S5 and S6) and the voltage-sensor domain (segments S1−S4) (*5*−*8*).

Calcium- and voltage-activated BK channels (known as MaxiK channels) also contain a S4 helix, but unlike K_v channels, they contain seven transmembrane helices (S0−S6) and a large cytosolic domain (S7−S10) (*9*). These channels are activated by both a voltage and cytoplasmic Ca^{2+}. They often colocalize with voltage-dependent calcium channels to dampen their excitatoric effect through negative feedback (*10*−*12*). The Ca^{2+} activation and the voltage activation act independently (*11*, *13*).

Within the voltage-sensor domain, the S4 segment is generally rich in Arg (or Lys) residues and forms a "paddle" motif with part of the S3 helix, S3b (*5*). This paddle motif provides a means for moving charges within the membrane and seems to be sensitive to the membrane potential (*5*, *14*). The gates of these proteins can thus be open or closed, depending on the voltage variations in the cell membrane. This voltage-sensor motif appears to be conserved within a wide range of channels (*15*−*19*). It has also been shown that the voltage-sensor motif can function as a voltage-activated proton channel without a separate pore domain (*17*−*19*). Crystal structures of several voltage-dependent potassium channels have been obtained, and the results have shown that the voltage-sensor paddle fragment, S3b−S4, moves within the membrane to open the pore (*5*−*8*, *20*−*22*). The crystal structures have further revealed that the paddle is composed of a helix−turn−helix motif. The paddle motif is rich in Arg residues, and the movement of these charges across the membrane is linked with pore gating (*23*, *24*). Many questions about the extent of the paddle motion within the membrane still remain, and different biophysical and biochemical techniques have been shown to give different results concerning the actual distance that the domain moves (*8*, *24*, *25*).

In this paper, we describe the high-resolution NMR solution structure of the voltage-sensor motif from the *Homo sapiens*

[†]This work was supported by The Swedish Research Council, The Carl Trygger Foundation, and the Magnus Bergvall Foundation.

[‡]The chemical shifts for HsapBK(233−260) in DPC micelles have been deposited in the BioMagResBank as entry 16112. The coordinates for the solution structure of HsapBK(233−260) in DPC micelles have been deposited in the Protein Data Bank as entry 2k44.

*To whom correspondence should be addressed. Phone: +46 8 162448. Fax: +46 8 155597. E-mail: lena.maler@dbb.su.se.

Published on Web 05/20/2009

BK K^+ channel, HsapBK(233−260).[1] It consists of 28 amino acid residues, with the sequence PVFVSVYLNRSWLGLRFLRALRLIQFSE. This sequence is totally conserved among BK channels of different types and from different species. On the other hand, the corresponding sequences in K_v channels appear not to be equally conserved, and hence, it is important to examine the structural differences and similarities between them. The membrane-bound structure of the fragment was obtained by reconstituting the peptide in dodecylphosphocholine (DPC) micelles. We demonstrate that the structure of the isolated motif does indeed fold into a helix−turn−helix motif. The structure will be helpful in future studies of the membrane interactions of the voltage-sensor motifs.

EXPERIMENTAL PROCEDURES

Sample Preparation. The voltage-sensor motif, HsapBK(233−260), was obtained as a custom synthesis from NeoMPS (Strasbourg, France) and used without further purification. Deuterated dodecylphosphocholine-d_{38} (DPC) was purchased from Cambridge Isotope Laboratories, Inc., while 1,2-dimyristoyl-*sn*-glycero-3-phosphocholine (DMPC-d_{54}) and 1,2-dihexanoyl-*sn*-glycero-3-phosphocholine (DHPC-d_{22}) were purchased from Avanti Polar Lipids, Inc. (Alabaster, AL).

For the ^{1}H NMR experiments and CD measurements, a sample containing 1 mM peptide was dissolved in 100 mM DPC-d_{38} (98%) and 50 mM potassium phosphate buffer (pH 5.5); 10% ^2H_2O was added for field/frequency lock stabilization in NMR experiments. A sample of 1 mM peptide in 300 mM, q = 0.25 (q is the concentration ratio of DMPC to DHPC) DMPC/DHPC bicelles was also prepared for CD measurements and initial NMR experiments. Bicelles were prepared by mixing lyophilized DMPC with a stock solution of DHPC (1 M) and phosphate buffer (final concentration of 50 mM, pH 5.8) to yield a total lipid concentration of 300 mM. Peptide dissolved in CH_3OH and $CHCl_3$ (1:3) was added to a freeze-dried bicelle solution; the mixture was freeze-dried yet again and subsequently dissolved in water.

CD Spectroscopy. CD spectra were recorded for HsapBK (233−260) in DPC and in a q = 0.25 DMPC/DHPC bicelle solution. CD measurements were acquired on a Chirascan CD spectrometer with a 0.1 mm quartz cell. The temperature was adjusted to 25 °C with a TC 125 temperature control. Wavelengths ranging from 190 to 250 nm were measured with a 1 nm step resolution. Spectra were collected and averaged over five measurements. Background spectra of the pure detergent solution and of the pure bicelle solution were subtracted from the peptide spectra.

Fluorescence Spectroscopy. Tryptophan fluorescence was measured on a Perkin-Elmer LS 50B luminescence spectrometer. All measurements where taken at room temperature in a quartz cuvette with a light path length of 2 mm. The excitation wavelength was 280 nm, and the emission was scanned from 300 to 500 nm. Ten scans were collected with a scan speed of 600 nm/min. The excitation bandwidth as well as the emission bandwidth was 10 nm.

NMR Spectroscopy. Two-dimensional ^{1}H NMR measurements were recorded on a Varian Inova spectrometer equipped with a triple-resonance probe head operating at a ^{1}H frequency of 800 MHz. Two-dimensional COSY (*26*, *27*), TOCSY (*28*), and NOESY (*29*) spectra were recorded for HsapBK(233−260) in 100 mM DPC. The TOCSY spectra were recorded with mixing times of 30, 55, and 80 ms, and the NOESY spectra were recorded with mixing times of 100, 150, and 300 ms. The 150 ms NOESY was used for assigning distance constraints, as described previously for structure determination of micelle-bound peptides (*30*). Spectra were typically collected as 2048−4096 × 320 data point matrices using 64−96 scans. Water suppression was achieved with the WATERGATE pulse sequence (*31*). The spectra were processed with NMRPipe version 2.3 (*32*), and spectral analysis was performed with Sparky 3 (*33*). All two-dimensional NMR experiments were performed at 37 °C.

Translational diffusion experiments were conducted on a Varian Inova spectrometer equipped with a triple-resonance probe head operating at a ^{1}H frequency of 600 MHz. Measurements were performed at 25 and 37 °C. Diffusion constants were determined for DPC in the monomer state using a 0.5 mM DPC sample, since the critical micelle concentration of DPC is 1 mM (*34*). Diffusion constants were measured using a modified Stejskal−Tanner spin−echo experiment (*35*−*37*) with a fixed diffusion time and a pulsed field gradient increasing linearly over 32 steps. To correct for field gradient inhomogeneity, the intensity decline for every experiment was fitted to a modified version of the Stejskal−Tanner equation (*38*). Viscosities of the samples were estimated by measuring the H_2O diffusion rates and comparing them to standard values in water (*39*), and the viscosity-corrected diffusion constants (*40*) could then be used to calculate hydrodynamic radii via the Stokes−Einstein relation using the assumption that the micelle is a hard sphere (*41*, *42*). A hydration layer with an estimated depth of 2.8 Å was assumed in the calculations.

Structure Calculation. Cross-peaks in the 150 ms mixing time NOESY spectrum were used for deriving distance constraints for calculating a solution structure for HsapBK(233−260) in DPC. In all, 327 distance constrains were assigned (160 intraresidue, 89 sequential, 72 medium-range, and 6 long-range constraints). The cross-peak intensities were initially converted to distances using routines in CYANA 2.0 (*43*). These distances were subsequently altered manually in several stages as described previously (*44*). Structures were generated using CYANA, applying standard annealing algorithms. Analyses of the structures, including analyses of secondary structure and backbone dihedral angles, were performed with PROCHECK NMR (*45*). A total of 100 structures were calculated, and a final ensemble of 25 structures was selected, on the basis of the CYANA target function, to represent the final solution structure. The coordinates of the final ensemble of structures have together with the distance constraints been deposited in the Protein Data Bank as entry 2k44. The chemical shift assignments have been deposited with the BMRB as entry 16112.

RESULTS

Interaction between HsapBK(233−260) and DPC. To determine the extent of structure in HsapBK(233−260) in various membrane mimetics, CD spectra were recorded between 190 and

[1]Abbreviations: HsapBK, *H. sapiens* BK K^+ channel; HsapBK(233−260), sequence P_{233}VFVSVYLNRSWLGLRFLRALRLIQFSE$_{260}$ derived from HsapBK; DPC, dodecylphosphocholine; CD, circular dichroism; NMR, nuclear magnetic resonance; NOESY, nuclear Overhauser effect spectroscopy; NOEs, proton−proton distances determined from NOESY cross-peaks; TOCSY, total correlation spectroscopy; rmsd, root-mean-square deviation; CMC, critical micelle concentration.

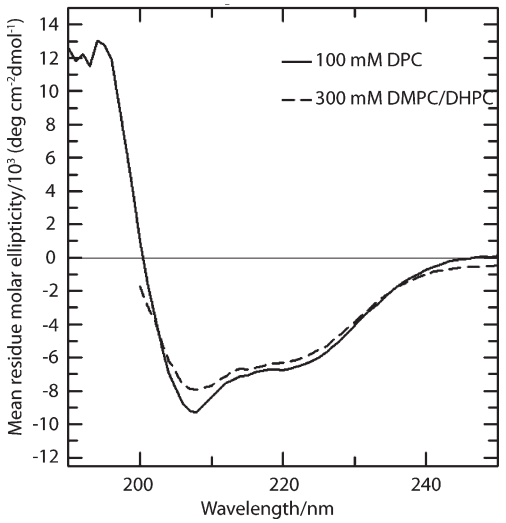

FIGURE 1: CD spectra recorded at 37 °C for 1 mM HsapBK(233−260) in 100 mM DPC (—) and in 300 mM, $q = 0.25$ DMPC/DHPC bicelles (– – –).

250 nm in 100 mM DPC and in a 300 mM DMPC/DHPC bicelle solution (Figure 1). Bicelles provide a bilayered environment, in which many proteins have been found to be active (*46*). It was difficult to measure the spectrum for the bicelle sample below 200 nm, and hence, only the spectrum between 200 and 250 nm is shown. This has previously been observed for peptides tightly bound to bicelles (*47*). It was also somewhat difficult to accurately measure the signal intensity for the peptide in the DPC sample below 195 nm.

Nevertheless, the spectra of the peptide in both $q = 0.25$ bicelle solution and DPC display the characteristic features of a helical structure, although the amplitude at 222 nm suggests that only ~30% of the sequence is structured. This may (in part) be due to difficulties in accurately estimating the peptide concentration. The similarity between the spectra indicates that the structure of the paddle motif is similar in the two membrane mimetic solvents, and that DPC provides an adequate membrane environment. Since the NMR spectra of the peptide in the bicelle solvent were hampered by large lipid signals and broad peptide resonances, DPC was subsequently chosen for performing the structural studies. The chemical shifts for the observable resonances in the peptide dissolved in the bicelle solution were, however, similar to those in DPC. Again, this indicates that the paddle fragment has a similar structure in DPC and in the bilayer bicelles.

The complex between DPC and the peptide was further analyzed by measuring translational diffusion coefficients for DPC as well as for the peptide at 25 and 37 °C (Table 1). The measurements at the lower temperature were made to ensure that the diffusion coefficients obtained at 37 °C were not influenced by a higher degree of convection currents in the sample. The calculated hydrodynamic radii did, however, not vary significantly within this temperature range.

The size of the peptide−DPC complex was examined from diffusion data. The peptide is only marginally soluble in aqueous solution and can thus be assumed to be fully bound to the DPC complex. Hence, on the basis of the diffusion rate of the peptide, a hydrodynamic radius of the DPC/peptide aggregates was calculated to 22.9 ± 0.3 Å at 37 °C.

To compare the size of the DPC/peptide aggregate to that of a DPC micelle, the size of the DPC micelle alone was estimated. A certain fraction of the DPC is dissolved as monomers in the solution, even above the CMC, and a weighted average between the monomer and the micelle diffusion is thus observed (*48*). Hence, we determined the diffusion rates for both monomeric DPC (below the CMC) and the DPC micelle sample. Using these values, we estimate that 3% of the total amount of DPC exists as free monomers and that the hydrodynamic radius for the DPC micelles without the peptide is 21.3 ± 0.3 Å, which corresponds well with previous results for DPC micelles (*49*, *50*).

Table 1: Diffusion Coefficients and Hydrodynamic Radii for DPC and HsapBK(233−260)

sample	D ($\times 10^{-11}$ m^2 s^{-1})[a] DPC	D ($\times 10^{-11}$ m^2 s^{-1})[a] HsapBK(233−260)	R_h (Å)[b]
	25 °C		
0.5 mM DPC	48.8 ± 0.3		1.9 ± 0.3
100 mM DPC	11.3 ± 0.2		20.6 ± 0.3
100 mM DPC and 1 mM HsapBK(233−260)	10.6 ± 0.1	9.3 ± 0.2	22.1 ± 0.4
	37 °C		
0.5 mM DPC	63.6 ± 0.4		2.4 ± 0.4
100 mM DPC	14.9 ± 0.2		21.3 ± 0.2
100 mM DPC and 1 mM HsapBK(233−260)	14.1 ± 0.4	12.8 ± 0.4	22.9 ± 0.4

[a] Normalized according to the diffusion of HDO to account for viscosity differences. [b] Hydrodynamic radius. For the DPC micelle sample, the fraction of free monomer in solution was taken into account. For the DPC−peptide complex, the radius was calculated from the peptide diffusion. The calculations have accounted for a hydration layer with an estimated depth of 2.8 Å.

Comparing the two, we see that adding the peptide to DPC corresponds to an increase in volume of ~25%, which is in agreement with similar studies of peptides in DPC micelles (*34*). The results show that the peptide forms a well-defined complex with the DPC molecules.

The intrinsic Trp fluorescence of Trp12 in HsapBK(233−260) was measured in DPC. A clear blue shift in the emission maximum as compared to what is expected for a solvent-exposed Trp residue was observed (341 nm for HsapBK(233−260) compared to 355 nm for a Trp residue in water) (*51*). This supports the diffusion results, and together with the fact that the peptide and micelle-bound DPC diffuse with the same diffusion constant, we conclude that the peptide is embedded in DPC. Very similar results have previously been observed for well-structured and tightly micelle-, bicelle-, or vesicle-bound peptides (*34*, *52*, *53*).

Solution Structure of HsapBK(233−260) in DPC. Two-dimensional COSY, NOESY, and TOCSY experiments were used to obtain resonance assignments for the peptide in DPC solution. In short, the assignment strategy was based on identifying spin systems in the TOCSY spectrum and connecting them together by sequential NOE patterns in the NOESY spectrum. The COSY spectrum was of little use, since the relatively broad peaks lead to cancellation of peaks. Approximately 90% of all ^{1}H atoms were assigned, including the side chain protons. Assignments for backbone H^N and H^α protons were found for all amino acid residues, except the N-terminal one. Most of the missing assignments were in side chains for which, e.g., H^β and H^γ protons overlapped. Secondary H^α chemical shifts were calculated according to the method of Wishart and Sykes (*54*) (Figure 2a).

For most of the peptide, secondary chemical shifts indicating helical structure are seen, with notable exceptions for residues Leu8, Asn9, and Gly14 and the termini. A solution structure for

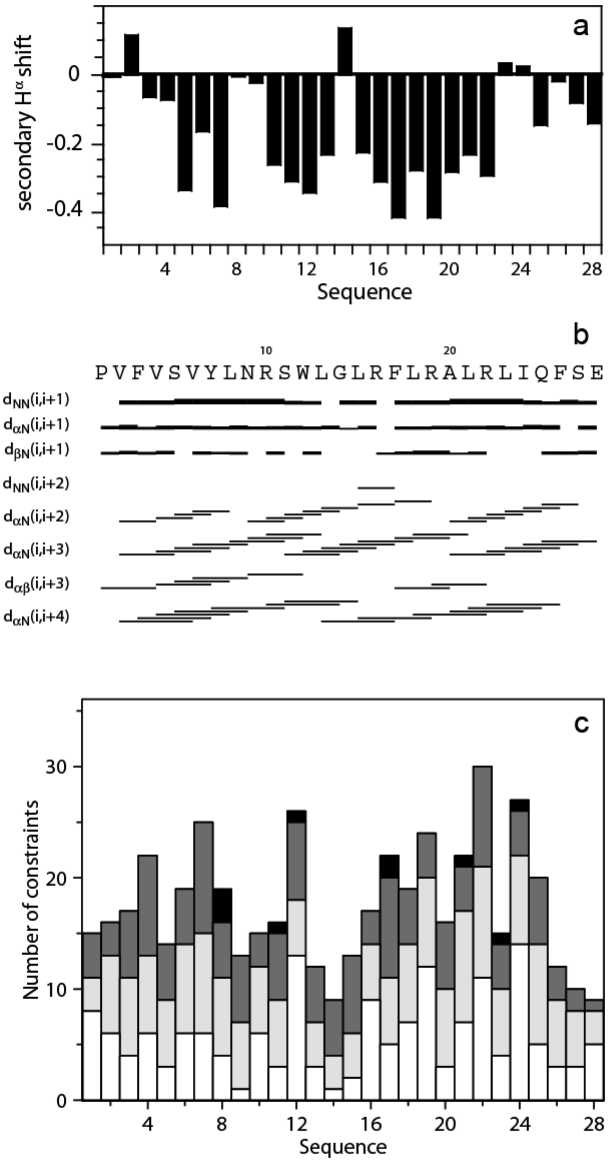

FIGURE 2: Structural data for HsapBK(233−260) in 100 mM DPC. (a) H^{α} secondary chemical shifts. (b) Summary of sequential and medium-range NOEs obtained from the NOESY spectrum recorded with a τ_{mix} of 150 ms. (c) Summary of the number of restraints for each amino acid residue: white for intraresidue, light gray for sequential, dark gray for medium-range, and black for long-range NOEs.

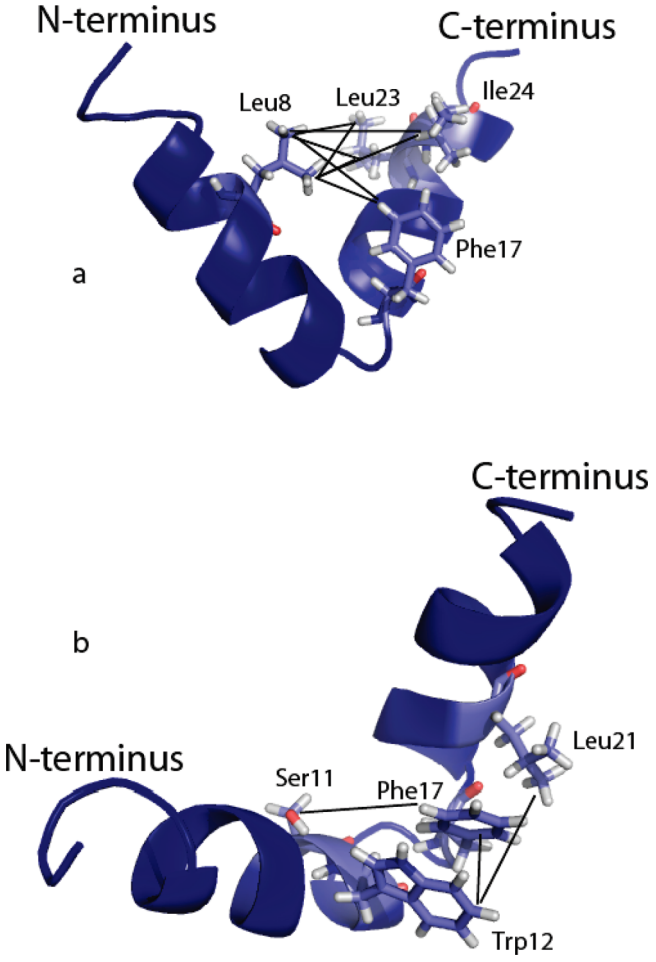

FIGURE 3: (a) Long-range NOEs were obtained between the methyl groups of Leu8 and the aromatic ring of Phe17 and the methyl groups of Leu23 and Ile24, respectively. (b) Long-range NOEs was also found between Trp12 and Phe17, between Trp12 and Leu21, and between Ser11 and Phe17.

the peptide was calculated on the basis of 327 distance constraints derived from the two-dimensional NOESY with a mixing time of 150 ms. In agreement with the helical secondary shifts, many of the medium-range NOEs indicating helical structure were found throughout the peptide, although several were missing in the region between Leu8 and Asn9, Trp12 and Arg19, and Leu23 and Glu28 (Figure 2b).

A summary of the number of constraints per residue is given in Figure 2c. A few (six) unambiguous long-range NOEs were found, which are essential for folding the structure into a helix−turn−helix motif. Part of a NOESY spectrum displaying some of these cross-peaks is shown in Figure S1 (Supporting Information). These NOEs are seen between Leu8, Ser11, and Trp12 and Phe17, Leu21, Leu23, and Ile24 (Figure 3a,b). From the final round of calculations, an ensemble of 25 structures was selected to represent the solution structure (Figure 4). These structures have low CYANA target function and modest distance violations (Table 2).

The presented structure was calculated on the basis of only six unambiguous long-range constraints. Furthermore, these were all set conservatively to an upper distance limit of 6 Å in the calculation. The interface of the two helices is not as well-defined as the secondary structure, but since the number of long-range constraints is so few compared to the number of sequential and medium-range constraints, this will not be reflected in the rmsd values for atomic coordinates. To visualize this, a picture in which the upper distance limit for the long-range NOEs is varied is included (Figure 5). As one can see, the overall structure is retained as the number of constraints is increased or decreased, but the relative position of the two helices is varied. Furthermore, each of the long-range NOEs has been carefully examined, so that none one of them forces a specific tertiary structure by itself, which can be a problem in the case of a sparse NOE network. We calculated the structure by using one distance constraint at a time, which showed that the fold was not created by enforcing one single distance (Figure S2 of the Supporting Information).

To further validate the structure, we carefully examined the calculated structure to ensure that no significant long-range constraints were missing in the data. In particular, we looked for potential long-range distances of <6 Å. On the basis of measured distances in the structure, the side chain of Val4 is close to both Leu23 and Ile24; however, the chemical shift of the two methyl groups in Val4 overlaps with that of one of the methyl

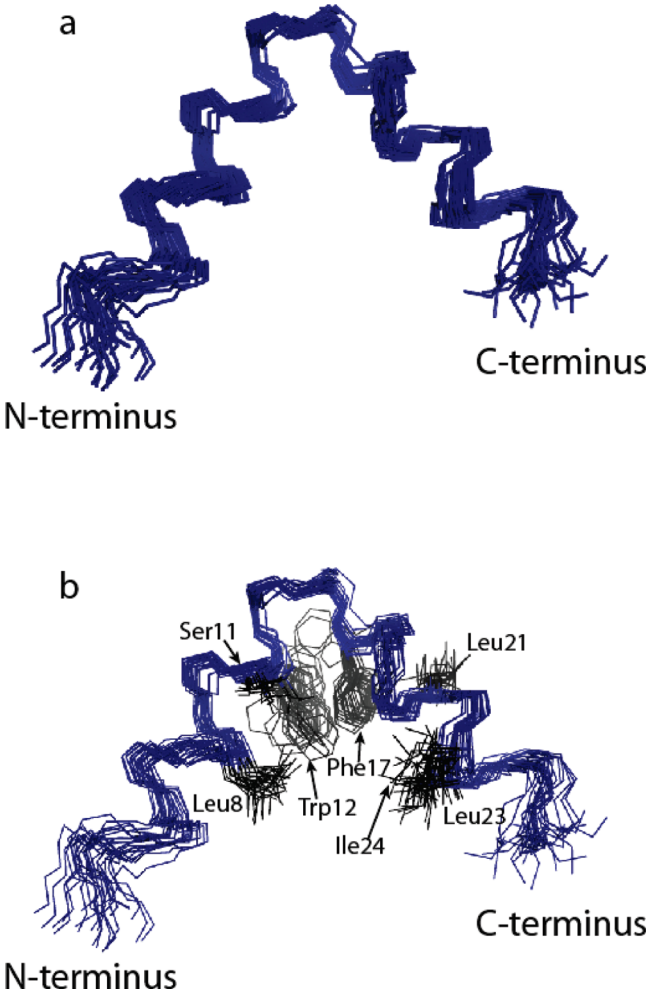

FIGURE 4: Solution structure of HsapBK(233−260) in 100 mM DPC as represented by an ensemble of the 25 structures with the lowest CYANA target function without (a) and with (b) the residues involved in long-range constraints. The structures were superimposed using backbone atoms in residues 5−14 and 18−26.

Table 2: Structural Statistics for the Ensemble of 25 Structures of HsapBK (233−260) in DPC Micelles

no. of constraints	327
Cyana target function	0.07 ± 0.03 Å^2
maximum distance violation	0.09 ± 0.04 Å
backbone atom rmsd (Å)	
all residues	0.83
residues 5−14	0.27
residues 18−26	0.14
residues 5−14, 18−26	0.60
Ramachandran plot regions (%)	
most favored	80.5
allowed region	18.2
generously allowed	1.3
disallowed	0

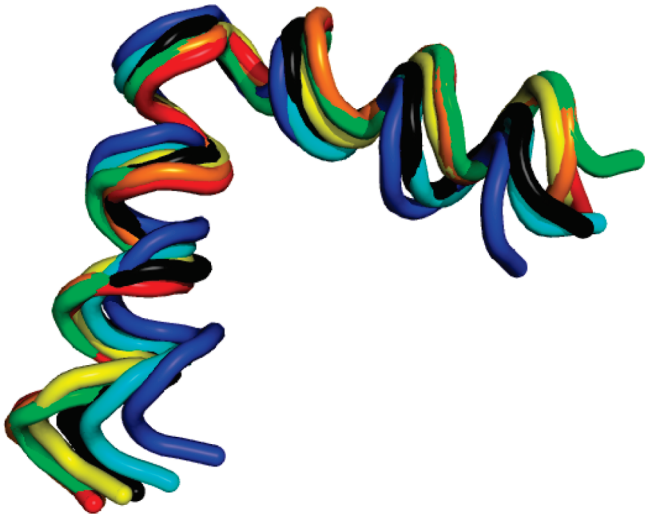

FIGURE 5: The interface between the two helices is not as well-defined as the secondary structure. To emphasize that, structures calculated with the long-range NOEs set to 5 Å (black), 5.5 Å (blue), 6 Å (cyan), 6.5 Å (green), 7 Å (yellow), 7.5 Å (orange), and 8 Å (red) are shown.

groups in Leu8 and in Leu18, and hence, we did not use these cross-peaks. The second unambiguously assigned methyl group resonance of Leu8 did, however, exhibit cross-peaks to Leu23, and this constraint was included.

Among other short distances between side chains in the structure, we note that Ser11 H^{β} protons are close to both Arg19 and Ala20 H^{β} protons. Cross-peaks corresponding to the chemical shifts of these protons can indeed be observed in the spectra, but the shifts of Arg19 and Ala20 overlap with other resonances in the peptide. Hence, no assignments were included.

Finally, several medium- and long-range distances between protons close to the turn of the structure should generate cross-peaks in the NOESY spectrum. Also here, the overlap is too severe to make unambiguous assignments. The overlap is mainly between methyl groups in Leu13 and Leu15 and between side chain protons in the Arg residues (Arg16 and Arg19). Gly14 had only very few inter-residue NOE cross-peaks (Figure 2c).

On the basis of analyses of backbone dihedral angles and the potential for forming helical hydrogen bonds, helical structure was assigned between residues Ser5 and Gly14 (N-terminal helix) and between Leu18 and Phe26 (C-terminal helix). Notably, the dihedral angles for Asn9 and Arg10 are not strictly α-helical. This is further supported by the lack of helical secondary shifts for these residues (Figure 2a) and may indicate a break in the N-terminal α-helix at this point. One should also note that residues 15−20 have dihedral angles within the α-helical region, but not in all structures within the ensemble. Analysis of the hydrogen bonding pattern was slightly more complicated. Regular α-helical hydrogen bonds, although weak, were found for most of the N-terminal helix, while hydrogen bonds were observed only for Ala20 with both Leu23 and Ile24, indicating the possibility of both NH(i)−O(i + 4) and NH(i)−O(i + 3) hydrogen bonding patterns. Hence, we conclude that the short C-terminal helix corresponding to S4 has irregular secondary structure, probably due to dynamic exchange between α-helical and 3_{10}-helical structure, but that the calculated backbone dihedral angles are within the α-helical region of the Ramachandran map for residues Leu18−Gln25.

The precision of the structure, as judged from rmsds in atomic coordinates, is fairly high, especially for the two helices (Table 2). The short turn between the two helices is defined by fewer distances, since NOE cross-peaks in this area are difficult to assign due to the extensive overlap in the spectrum (Figure 2c).

DISCUSSION

In this report, we have determined the solution structure of the putative S3b−S4 voltage-sensor paddle in the

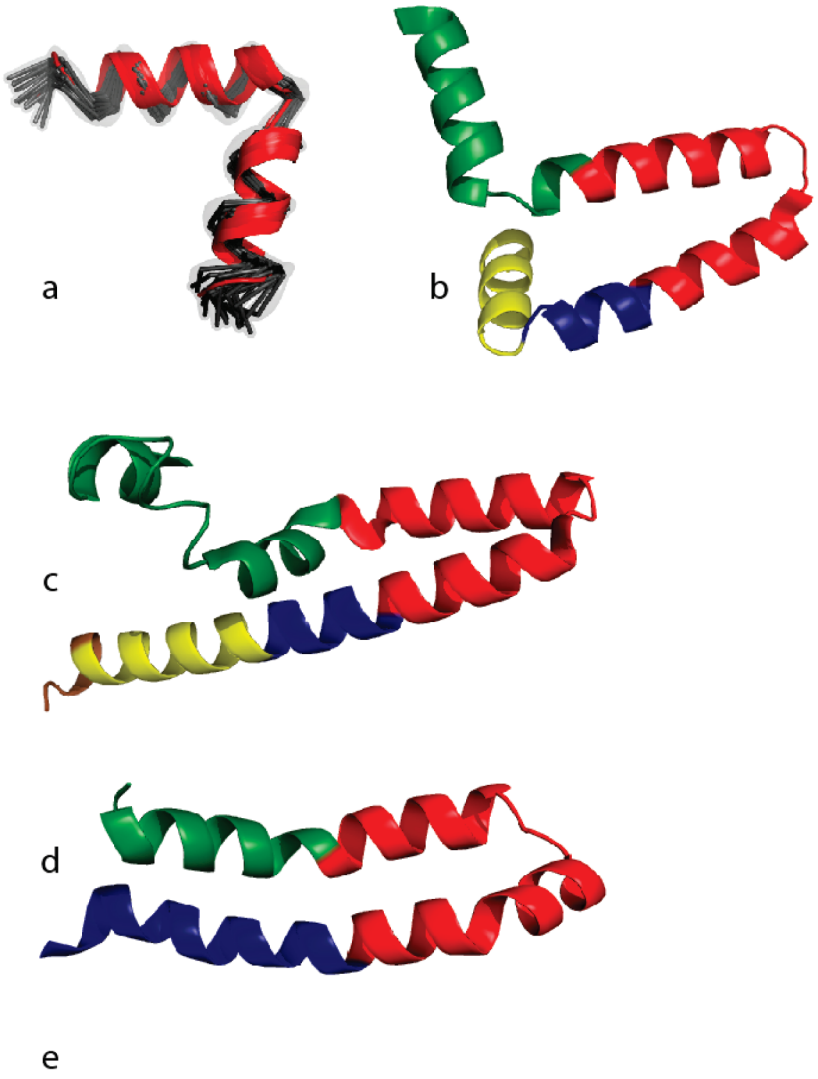

FIGURE 6: Comparison of the S3b−S4 sequence in HsapBK with the corresponding sequences from K_vAP and K_v1.2 channels. An overlay of all 25 structures for HsapBK(233−260) in the NMR-derived ensemble with the average structure colored red is shown in panel a. Panel b shows the S3−S4 fragment in the K_vAP structure (PDB entry 1ORQ). Panel c is from the structure of the isolated sensor in K_vAP (PDB entry 1ORS). Panel d shows the structure of the S3−S4 sequence in the rat K_v2.1 paddle chimera channel (PDB entry 2R9R). The region corresponding to the HsapBK S3b−S4 fragment is colored red in all structures. Connecting regions in the other structures are shown in different colors to facilitate comparison. A multiple-sequence alignment of the four sequences is shown in panel e, with the same color coding that is used in panels a−d. Completely conserved residues are marked with asterisks. Notably, the turn in the K_v2.1 channel is located in a different position than in the other structures.

voltage- and calcium-dependent HsapBK potassium channel. The isolated paddle in DPC micelles is here shown to form a structure in which two short helices interact to form a helix−turn−helix motif. On the basis of previous sequence alignments between the S3b−S4 motif in HsapBK and the K_vAP potassium channels, it is anticipated that the S3b helix spans residues 1−10 and that the S4 helix spans residues 12−27 (*5*) in HsapBK. In this study, we see that the N-terminal helix (corresponding to S3) of HsapBK(233−260) comprises residues Ser5−Gly14 and that the C-terminal helix (corresponding to S4) comprises residues Leu18−Phe26, although there is evidence, from both secondary chemical shifts and NOEs, that the C-terminal helix may comprise also residues preceding these (Leu15−Phe17).

Comparison of the structure of the HsapBK segment to those of crystal structures of K_v channels (*5*, *7*, *8*) shows that they are in part similar (Figure 6). The hydrophobic interactions between the two helices in this structure mainly involve Leu8, Ser11, Trp12, Phe17, Leu21, Leu23, and Ile24. Compared with other BK channels in different species, all residues in S3 and S4 in the proteins are completely conserved (*55*). Compared with the Shaker and K_v or Na_v channels, these residues are conservatively replaced with other aromatic and hydrophobic residues (*5*, *6*, *55*). However, Trp12 that participates in the

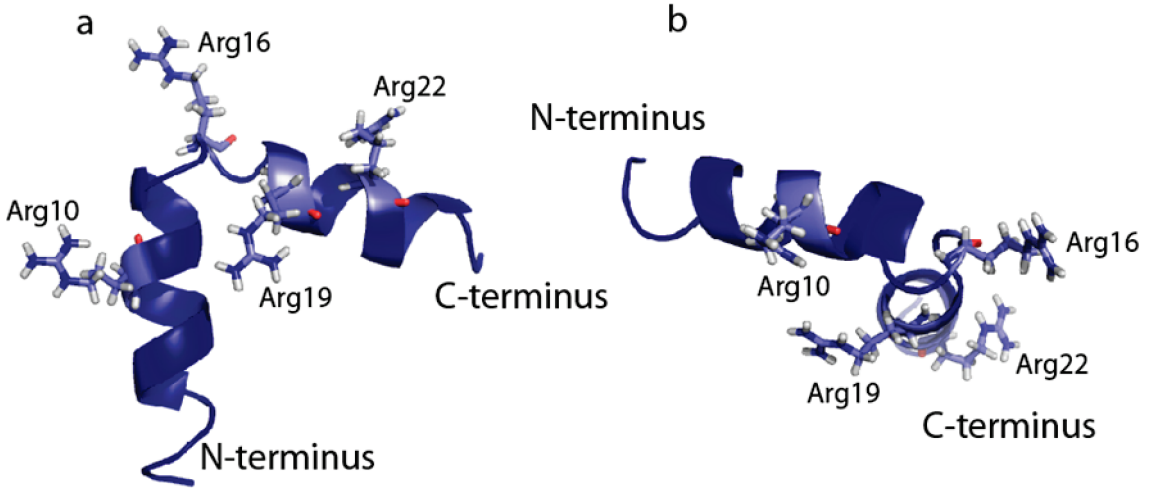

FIGURE 7: Solution structure of HsapBK(233−260). The side chains of the four Arg residues are shown. Panel a shows a front view, while panel b shows a view down along the C-terminal S4 helix, indicating that the Arg residues are all on the outside of the structure.

long-range contacts in this structure is not conserved in the K_vAP and $K_v1.2$ S3−S4 fragments (Figure 6). Furthermore, Gly14 in HsapBK(233−260) is located in the loop between the two helices and hence corresponds to the glycine-rich loop in K_vAP(112−146) and not to the S4 segment as suggested from ClustalW alignment (*5*). This is not a surprise, since structure is more evolutionarily conserved than primary sequence. The two helices in the HsapBK(233−260) structure presented here are much shorter, and not as well-packed as in other K_v structures. The K_v channels are predicted to have several residues in a loop region between the two helices, while this is not the case for BK channels. The S3b−S4 region of the human BK channels is furthermore predicted to be shorter than in the K_v channels.

As there are no structures of a full-length BK channel, we cannot determine whether the differences observed here are due to the DPC environment or the lack of the remaining protein or if they indeed are true differences. It is, however, important to note that this short fragment does indeed form a helix−turn−helix structure in the presence of a membrane mimetic and that the location of the S3b−S4 domain may differ somewhat in BK channels as compared to K_v channels, while the structural feature of the paddle is conserved.

It has been demonstrated that the voltage sensors can function on their own, in proteins without ion-conducting pores (*17*−*19*, *56*), and that the paddle domains in K_v and Na_v channels are modular and can be swapped between different ion channels (*57*−*59*). This supports the idea that the structure presented here represents a nativelike conformation of the paddle domain in BK channels.

The structure is embedded within a layer of DPC molecules, as evidenced from diffusion measurements, which serve as a model for the membrane. Several solution structures of membrane proteins and peptides in DPC, as well as in other detergents, have been determined (*34*, *44*, *60*−*62*), indicating that the DPC provides a reasonable environment for investigating structure. Many proteins retain their nativelike structure and activity in such solvents. It should, however, be said that there are also protein fragments that do not adopt their native structure in micellar environments. These are often surface-associated protein motifs, or peptides (*44*, *62*), for which the structure depends critically on the membrane surface.

The four Arg residues within the peptide have been implicated in the gating properties of the voltage-sensor motif, which has been shown by various biophysical techniques (*23*−*25*, *63*). The extent to which these Arg residues move across the lipid bilayer has, however, been debated. MacKinnon's group has shown that the paddle is highly mobile (*63*). Furthermore, the crystal structure of a chimaeric channel in a lipid environment revealed that the charges are exposed to the lipid phosphates in the membrane, and that charge stabilization may occur through interactions with negatively charged residues (*8*). It has also been demonstrated that the isolated S4 helix from K_vAP, containing most of the Arg residues, can be inserted in a membrane in a transmembrane way and that the charges are stabilized by interactions with the lipid phosphates (*64*, *65*). Molecular dynamics simulations of the voltage-sensor domain have shown that at least some of the Arg residues in the voltage-sensor domain are not exposed to the hydrophobic interior of the bilayer (*66*−*68*). It has been suggested that the paddle undergoes considerable motion and that the gating involves changing the bilayer and water exposure of the S3b−S4 paddle (*66*). It has also been shown that the membrane may be affected by the sensor, leading to a decrease in the hydrophobic thickness of the bilayer (*66*, *69*). Here we see that three of the Arg residues are located in the putative S4 part of the fragment, and all are more or less exposed on the surface of the structure (Figure 7). The fourth Arg residue is situated close to the C-terminus of the N-terminal helix, and its side chain is also exposed. This may in part be due to the nature of the membrane mimetic but still shows that the fragment forms a structure with exposed Arg residues.

Another interesting observation is that the C-terminal helix in HsapBK(233−260), corresponding to S4, seems to be able to adopt (partially) a 3_{10}-helical conformation. This has been implicated in being part of the gating mechanism (*8*, *66*, *69*, *70*), in which the change in conformation is associated with the movement between the resting and activated states.

The solution structure of the sequence derived from the HsapBK channel in this investigation clearly shows that a helix−turn−helix conformation is formed and that further studies of the motion and membrane interactions of this motif in more nativelike membrane environments, such as phospholipid bicelles, are feasible. Future studies of mobility and, in particular, the response to membrane potential will together with

the structure presented here reveal important insights into the dynamics of this sequence and of movements within a bilayer and reveal details in membrane interactions of the voltage-sensor paddle.

ACKNOWLEDGMENT

We thank the Swedish NMR Centre for access to the NMR spectrometers.

SUPPORTING INFORMATION AVAILABLE

Figures showing parts of a two-dimensional NOESY spectrum and the result of individual long distance constraints on the structure. This material is available free of charge via the Internet at http://pubs.acs.org.

REFERENCES

(1) Hodgin, A. L., and Huxley, A. F. (1952) A Quantitative Description of Membrane Current and its Application to Conduction and Excitation in Nerve. *J. Physiol. 117, 500–544*.
(2) Jan, L. Y., and Jan, Y. N. (1997) Voltage-Gated and Inwardly Rectifying Potassium Channels. *J. Physiol. 505 (Part 2), 267–282*.
(3) Miller, C. (2000) An Overview of the Potassium Channel Family. *Genome Biol. 1, 0004.1–0004.5*.
(4) Bezanilla, F. (2000) The Voltage Sensor in Voltage-Dependent Ion Channels. *Physiol. Rev. 80, 555–592*.
(5) Jiang, Y., Lee, A., Chen, J., Ruta, V., Cadene, M., Chait, B. T., and MacKinnon, R. (2003) X-ray Structure of a Voltage-Dependent K Channel. *Nature 423, 33–41*.
(6) Long, S. B., Campbell, E. B., and Mackinnon, R. (2005) Crystal Structure of a Mammalian Voltage-Dependent Shaker Family K^+ Channel. *Science 309, 897–903*.
(7) Lee, S. Y., Lee, A., Chen, J., and MacKinnon, R. (2005) Structure of the KvAP Voltage-Dependent K^+ Channel and its Dependence on the Lipid Membrane. *Proc. Natl. Acad. Sci. U.S.A. 102, 15441–15446*.
(8) Long, S. B., Tao, X., Campbell, E. B., and MacKinnon, R. (2007) Atomic Structure of a Voltage-Dependent K^+ Channel in a Lipid Membrane-Like Environment. *Nature 450, 376–382*.
(9) Meera, P., Wallner, M., Song, M., and Toro, L. (1997) Large Conductance Voltage- and Calcium-Dependent K^+ Channel, a Distinct Member of Voltage-Dependent Ion Channels with Seven N-Terminal Transmembrane Segments (S0-S6), an Extracellular N Terminus, and an Intracellular (S9-S10) C Terminus. *Proc. Natl. Acad. Sci. U.S.A. 94, 14066–14071*.
(10) Marty, A. (1981) Ca-Dependent K Channels with Large Unitary Conductance in Chromaffin Cell Membranes. *Nature 291, 497–500*.
(11) Pallotta, B. S., Magleby, K. L., and Barrett, J. N. (1981) Single Channel Recordings of Ca^{2+}-Activated K^+ Currents in Rat Muscle Cell Culture. *Nature 293, 471–474*.
(12) Latorre, R., Vergara, C., and Hidalgo, C. (1982) Reconstitution in Planar Lipid Bilayers of a Ca^{2+}-Dependent K^+ Channel from Transverse Tubule Membranes Isolated from Rabbit Skeletal Muscle. *Proc. Natl. Acad. Sci. U.S.A. 79, 805–809*.
(13) Ghatta, S., Nimmagadda, D., Xu, X., and O'Rourke, S. T. (2006) Large-Conductance, Calcium-Activated Potassium Channels: Structural and Functional Implications. *Pharmacol. Ther. 110, 103–116*.
(14) Bezanilla, F. (2002) Voltage Sensor Movements. *J. Gen. Physiol. 120, 465–473*.
(15) Noda, M., Ikeda, T., Suzuki, H., Takeshima, H., Takahashi, T., Kuno, M., and Numa, S. (1986) Expression of Functional Sodium Channels from Cloned cDNA. *Nature 322, 826–828*.
(16) Murata, Y., Iwasaki, H., Sasaki, M., Inaba, K., and Okamura, Y. (2005) Phosphoinositide phosphatase activity coupled to an intrinsic voltage sensor. *Nature 435, 1239–1243*.
(17) Ramsey, I. S., Moran, M. M., Chong, J. A., and Clapham, D. E. (2006) A Voltage-Gated Proton-Selective Channel Lacking the Pore Domain. *Nature 440, 1213–1216*.
(18) Sasaki, M., Takagi, M., and Okamura, Y. (2006) A Voltage Sensor-Domain Protein is a Voltage-Gated Proton Channel. *Science 312, 589–592*.
(19) Tombola, F., Ulbroch, M. H., and Isacoff, E. Y. (2008) The voltage-gated proton channel Hv1 has two pores, each controlled by one voltage sensor. *Neuron 58, 546–556*.
(20) Doyle, D. A., Cabral, J. M., Pfuetzner, R. A., Kuo, A., Gulbis, J. M., Cohen, S. L., Chait, B. T., and MacKinnon, R. (1998) The Structure of the Potassium Channel: Molecular Basis of K Conduction and Selectivity. *Science 280, 69*.
(21) Jiang, Y., Lee, A., Chen, J., Cadene, M., Chait, B. T., and MacKinnon, R. (2002) The Open Pore Conformation of Potassium Channels. *Nature 417, 523–526*.
(22) Kuo, A., Gulbis, J. M., Antcliff, J. F., Rahman, T., Lowe, E. D., Zimmer, J., Cuthbertson, J., Ashcroft, F. M., Ezaki, T., and Doyle, D. A. (2003) Crystal Structure of the Potassium Channel KirBac1.1 in the Closed State. *Science 300, 1922–1926*.
(23) Jiang, Y., Ruta, V., Chen, J., Lee, A., and MacKinnon, R. (2003) The Principle of Gating Charge Movement in a Voltage-Dependent K Channel. *Nature 423, 42–48*.
(24) Cuello, L. G., Cortes, D. M., and Perozo, E. (2004) Molecular Architecture of the KvAP Voltage-Dependent K^+ Channel in a Lipid Bilayer. *Science 306, 491–495*.
(25) Posson, D. J., Ge, P., Miller, C., Bezanilla, F., and Selvin, P. R. (2005) Small vertical movement of a K channel voltage sensor measured with luminescence energy transfer. *Nature 436, 848–851*.
(26) Jeener, J. (1971) Thesis, Ampere Summer School, Basko Polje, Yugoslavia.
(27) Aue, W., Bartholdi, E., and Ernst, R. (1976) Two-Dimensional Spectroscopy. Application to Nuclear Magnetic Resonance. *J. Chem. Phys. 64, 2229*.
(28) Braunschweiler, L., and Ernst, R. R. (1983) Coherence Transfer by Isotropic Mixing: Application to Proton Correlation Spectroscopy. *J. Magn. Reson. 53, 8*.
(29) Jeener, J., Meier, B. H., Bachmann, P., and Ernst, R. R. (1979) Investigation of Exchange Processes by Two-Dimensional NMR Spectroscopy. *J. Chem. Phys. 71, 4546–4553*.
(30) Papadopoulos, E., Oglecka, K., Mäler, L., Jarvet, J., Wright, P. E., Dyson, H. J., and Gräslund, A. (2006) NMR solution structure of the peptide fragment 1−31, derived from unprocessed mouse doppel protein, in DHPC micelles. *Biochemistry 45, 159–166*.
(31) Piotto, M., Saudek, V., and Sklenár, V. (1992) Gradient-Tailored Excitation for Single-Quantum NMR Spectroscopy of Aqueous Solutions. *J. Biomol. NMR 2, 661–665*.
(32) Delaglio, F., Grzesiek, S., Vuister, G. W., Zhu, G., Pfeifer, J., and Bax, A. (1995) NMRPipe: A Multidimensional Spectral Processing System Based on UNIX Pipes. *J. Biomol. NMR 6, 277–293*.
(33) Goddard, T. D., and Kneller, D. G. (1999) Sparky 3, University of California, San Francisco.
(34) Kallick, D. A., Tessmer, M. R., Watts, C. R., and Li, C. Y. (1995) The use of Dodecylphosphocholine Micelles in Solution NMR. *J. Magn. Reson., Ser. B 109, 60–65*.
(35) Stejskal, E. O., and Tanner, J. E. (1965) Spin Diffusion Measurements: Spin Echoes in the Presence of a Time Dependent Field Gradient. *J. Chem. Phys. 42, 288–292*.
(36) von Meerwall, E., and Kamat, M. (1989) Effect of Residual Field Gradients on Pulsed Gradient NMR Diffusion Measurements. *J. Magn. Reson. 83, 309–323*.
(37) Callaghan, P., Komlosh, M., and Nydén, M. (1998) High Magnetic Field Gradient PGSE NMR In the Presence of a Large Polarizing Field. *J. Magn. Reson. 133, 177–182*.
(38) Damberg, P., Jarvet, J., and Gräslund, A. (2001) Accurate Measurement of Translational Diffusion Coefficients: A Practical Method to Account for Nonlinear Gradients. *J. Magn. Reson. 148, 343–348*.
(39) Longsworth, L. G. (1960) The Mutual Diffusion of Light and Heavy Water. *J. Phys. Chem. 64, 1914–1917*.
(40) Andersson, A., Almqvist, J., Hagn, F., and Mäler, L. (2004) Diffusion and dynamics of penetratin in different membrane mimicking media. *Biochim. Biophys. Acta 1661, 18–25*.
(41) Price, W. S. (1997) Pulsed-field gradient nuclear magnetic resonance as a tool for studying translational diffusion: Part 1. Basic theory. *Concepts Magn. Reson. 9, 299–336*.
(42) Cantor, C. R., and Schimmel, P. R. (1980) Biophysical Chemistry, W. H. Freeman, San Fransisco.
(43) Guntert, P., Mumenthaler, C., and Wuthrich, K. (1997) Torsion Angle Dynamics for NMR Structure Calculation with the New Program DYANA. *J. Mol. Biol. 273, 283–298*.
(44) Andersson, A., and Mäler, L. (2002) NMR Solution Structure and Dynamics of Motilin in Isotropic Phospholipid Bicellar Solution. *J. Biomol. NMR 24, 103–112*.
(45) Laskowski, R. A., MacArthur, M. W., Moss, D. S., and Thornton, J. M. (1993) PROCHECK: A Program to Check the Stereochemical Quality of Protein Structures. *J. Appl. Crystallogr. 26, 283–291*.
(46) Sanders, C. R., and Sonnichsen, F. (2006) Solution NMR of Membrane Proteins: Practice and Challenges. *Magn. Reson. Chem. 44, S24–S40*.

(47) Lind, J., Nordin, J., and Maler, L. (2008) Lipid Dynamics in Fast-Tumbling Bicelles with Varying Bilayer Thickness: Effect of Model Transmembrane Peptides. *Biochim. Biophys. Acta 1778, 2526–2534*.
(48) Lindman, B., Puyal, M., Kamenka, N., Rymdén, R., and Stilbs, P. (1984) Micelle Formation of Anionic and Cationic Surfactants from Fourier Transform Hydrogen-1 and Lithium-7 Nuclear Magnetic Resonance and Tracer Self-Diffusion Studies. *J. Phys. Chem. 88, 5048–5057*.
(49) Lauterwein, J., Bosch, C., Brown, L. R., and Wuthrich, K. (1979) Physicochemical Studies of the Protein-Lipid Interactions in Melittin-Containing Micelles. *Biochim. Biophys. Acta 556, 244–264*.
(50) Gao, X., and Wong, T. C. (1998) Studies of the Binding and Structure of Adrenocorticotropin Peptides in Membrane Mimics by NMR Spectroscopy and Pulsed-Field Gradient Diffusion. *Biophys. J. 74, 1871–1888*.
(51) Lakowicz, J. R. (1999) Principles of Fluorescence Spectroscopy, Kluwer Academic Press, New York.
(52) Bárány-Wallje, E., Andersson, A., Gräslund, A., and Mäler, L. (2006) Dynamics of Transportan in Bicelles is Surface Charge Dependent. *J. Biomol. NMR 35, 137–147*.
(53) Magzoub, M., Kilk, K., Eriksson, L. E. G., Langel, U., and Gräslund, A. (2001) Interaction and structure induction of cell-penetrating peptides in the presence of phospholipid vesicles. *Biochim. Biophys. Acta 1512, 77–89*.
(54) Wishart, D. S., and Sykes, B. D. (1994) Chemical Shifts as a Tool for Structure Determination. *Methods Enzymol. 239, 363–392*.
(55) Ma, Z., Wong, K. Y., and Horrigan, F. T. (2008) An extracellular Cu^{2+} binding site in the voltage sensor of BK and Shaker potassium channels. *J. Gen. Physiol. 131, 483–502*.
(56) Freites, J. F., Tobias, D. J., and White, S. H. (2006) A voltage-sensor water pore. *Biophys. J. 91, L90–L92*.
(57) Alabi, A. A., Bahamonde, M. I., Jung, H. J., Kim, J. I., and Swartz, K. J. (2007) Portability of paddle motif function and pharmacology in voltage sensors. *Nature 450, 370–375*.
(58) Bosmans, F., Martin-Euclaire, M.-F., and Swartz, K. J. (2008) Deconstructing voltage sensor function and pharmacology in sodium channels. *Nature 456, 202–208*.
(59) Swartz, K. J. (2008) Sensing voltage across lipid membranes. *Nature 456, 891–897*.
(60) Arora, A., Abildgaard, F., Bushweller, J. H., and Tamm, L. K. (2001) Structure of Outer Membrane Protein A Transmembrane Domain by NMR Spectroscopy. *Nat. Struct. Biol. 8, 334–338*.
(61) Tamm, L. K., and Liang, B. (2006) NMR of Membrane Proteins in Solution. *Prog. Nucl. Magn. Reson. Spectrosc. 48, 201–210*.
(62) Chou, J. J., Kaufman, J. D., Stahl, S. J., Wingfield, P. T., and Bax, A. (2002) Micelle-Induced Curvature in a Water-Insoluble HIV-1 Env Peptide Revealed by NMR Dipolar Coupling Measurement in Stretched Polyacrylamide Gel. *J. Am. Chem. Soc. 124, 2450–2451*.
(63) Ruta, V., Chen, J., and MacKinnon, R. (2005) Calibrated Measurement of Gating-Charge Arginine Displacement in the KvAP Voltage-Dependent K^+ Channel. *Cell 123, 463–475*.
(64) Hessa, T., White, S. H., and von Heijne, G. (2005) Membrane insertion of a potassium-channel voltage sensor. *Science 307, 1427–1427*.
(65) Freites, J. A., Tobias, D. J., von Heijne, G., and White, S. H. (2005) Interface connections of a transmembrane voltage sensor. *Proc. Natl. Acad. Sci. U.S.A. 102, 15059–15064*.
(66) Sands, Z. A., Grottesi, A., and Sansom, M. S. P. (2006) The intrinsic flexibility of the Kv voltage sensors and its implications for channel gating. *Biophys. J. 90, 1598–1606*.
(67) Treptow, W., and Tarek, M. (2006) Environment of the gating charges in the Kv1.2 Shaker potassium channel. *Biophys. J. 90, L64–L66*.
(68) Jogini, V., and Roux, B. (2007) Dynamics of the Kv1.2 voltage-gated K^+ channel in a membrane environment. *Biophys. J. 93, 3070–3082*.
(69) Bjelkmar, P., Niemelä, P. S., Vattulainen, I., and Lindahl, E. (2009) Conformational changes and slow dynamics through microsecond polarized atomistic molecular simulation of an integral Kv1.2 ion channel. *PLoS Comput. Biol. 5, No. e1000289*.
(70) Villalba-Galea, C. A., Sandtner, W., Starace, D. M., and Bezanilla, F. (2008) S4-based voltage sensors have three major conformations. *Proc. Natl. Acad. Sci. U.S.A. 105, 17600–17607*.

I. Membrane-based Induction of α-helical Structure within a Subset of Peptides Derived from HAMP domains

Membrane-based induction of α-helical structure within a subset of peptides derived from HAMP domains

Sofia Unnerståle[1], Gunnar von Heijne[1], Roger R. Draheim[1,2]* and Lena Mäler[1]*

[1]Department of Biochemistry and Biophysics, Arrhenius Laboratories for Natural Sciences, Stockholm University, Stockholm, Sweden; [2]Current address: Institute for Biochemistry, Johann Wolfgang Goethe University, Frankfurt am Main, Germany

Running Title: Induction of α-helical structure in HAMP peptides

*Corresponding authors (R. R. D. and L.M.):

Department of Biochemistry and Biophysics
Stockholm University
Svante Arrhenius väg 16
10691 Stockholm
Sweden
Tel: +46 8 16 2448
Fax: +46 8 15 5597
Email: rogerdraheim@gmail.com, lena@dbb.su.se

Abstract

HAMP domains connect extracellular stimulus-sensing domains with the cytoplasmic domains responsible for intracellular signal generation. These domains are composed of two amphipathic sequences (AS1 and AS2) predicted to form α-helices joined by a non-helical connector. Within the context of prokaryotic membrane-spanning receptors, these domains are usually found adjacent to the inner leaflet of the cytoplasmic membrane. Because of this close proximity, we examined the influence of several membrane mimetics on peptides containing either AS1 or AS2 from four different HAMP domains: the *Archaeoglobus fulgidus* protein (Af1503), the *E. coli* osmosensor ($EnvZ_{Ec}$), the *E. coli* nitrate/nitrite sensor ($NarX_{Ec}$) and the aspartate chemoreceptor of *E. coli* (Tar_{Ec}). Far-UV CD was employed to estimate the induction of secondary structure upon addition of zwitterionic or negatively-charged large unilamellar vesicles (LUVs). In the case of AS1 from $NarX_{Ec}$, a significant (~ 3-fold) increase in the α-helical character upon adding negatively charged LUVs was observed. A significant (~ 5-fold) increase in α-helical character within AS1 from Tar_{Ec} was observed upon addition of zwitterionic LUVs, and a further induction (~ 8-fold in total) was observed upon addition of negatively-charged LUVs. We also quantified the extent of interaction between peptides and bicelles with similar lipid compositions. Both AS1 from $NarX_{Ec}$ and from Tar_{Ec} were seen to interact with phospholipid bicelles, while AS1 from Af1503 and $EnvZ_{Ec}$ failed to interact to a similar extent. Based on these results, we propose that a correlation exists between the mechanism of transmembrane communication employed by an intact receptor and the propensity for membrane-induced α-helicity in AS1. We conclude by hypothesizing how modulation of AS1 α-helicity could contribute to signal transduction by HAMP domains.

Keywords: HAMP domain, signal transduction, transmembrane communication, α-helicity of AS1, membrane-spanning receptors

HAMP domains[1] are found adjacent to the inner leaflet of the cytoplasmic membrane within many prokaryotic membrane-spanning receptors[2], including several well-characterized sensor histidine kinases (SHKs) and methyl-accepting chemotaxis proteins (MCPs), which are often referred to as chemoreceptors. These domains are responsible for converting extracellular sensory input into an intracellular signaling response within more than 7500 proteins[3]. HAMP domains were originally identified as "linker" sequences between the second transmembrane helix (TM2) of the membrane-spanning serine chemoreceptor of *E. coli* (Tsr_{Ec}) and the cytoplasmic domain responsible for signal propagation[4]. A subsequent bioinformatic analysis demonstrated that similar "linker" regions exist within four protein families: histidine kinases, adenlyate cyclases, methyl-accepting chemotaxis proteins and phosphatases[1]. While HAMP domains possess little conservation at the residue level, they remain highly-conserved at the level of secondary structure, consisting of two amphipathic sequences (AS1 and AS2) predicted to form α-helices joined by a non-helical connector (CTR)[1,5,6].

Within the context of prokaryotic membrane-spanning receptors, several recent models for signal transduction by HAMP domains have been proposed. The first model, commonly referred to as the "gearbox" model, is based upon the sole high-resolution three-dimensional structure of a HAMP domain[3]. This model proposes that the observed parallel four-helix bundle is able to shift between conformations consistent with different signaling states by alternating between the structurally-observed "complementary *x-da*" configuration, also known as knobs-to-knobs packing, and the more typical knobs-into-holes "*a-d* pairing". Interconversion between these configurations is suggested to be facilitated by a concerted rotation of approximately 26 degrees of relatively rigid helices. It should be noted that while this initial high-resolution three-dimensional structure is illuminating, the authors were only able to resolve the noncanonical knobs-into-knobs or "complementary *x-da*" configuration, and failed to experimentally determine the other[3]. Subsequent studies determined that HAMP domains within intact receptors responsible for mediating aerotaxis (Aer_{Ec})[7], aspartate[8], or serine[9] chemotaxis (Tar_{Ec} and Tsr_{St}) appeared to form a parallel four-helix bundle consistent with the high-resolution structure[3]. However, further experimentation within these intact receptors resulted in the proposal of other possible intradimer signal-transducing mechanisms. These mechanisms include a "scissors"-type model that pivots the individual HAMP subunits relative to one another based on disulfide-mapping within Tar_{St}[8] and a "dynamic bundle" model that invokes changes in the overall stability of the four-helix bundle based on mutagenic analysis of Tsr_{Ec}[9]. Finally, cryo-electron tomography and subsequent three-dimensional averaging demonstrated an interdimer shift between "compact" and "expanded" packing of the three HAMP domains within a homohexameric trimer-of-dimers composed solely of Tsr_{Ec}[10]. It should be noted that these models need not be mutually exclusive.

Even though HAMP domains are often found in a membrane-proximal location, none of these studies directly analyze the potential contribution of the membrane to the overall character of these domains. Therefore, based on part of a

larger project aimed at understanding the importance of receptor-membrane interactions, we characterized the interactions between peptides consisting of either AS1 or AS2 from a subset of well-characterized prokaryotic membrane-spanning receptors and various membrane mimetics *in vitro*. In the work presented here, we examined peptides containing AS1 or AS2 sequences from the previously-characterized *Archaeoglobus fulgidus* protein Af1503 because it was used to determine the high-resolution three-dimensional structure[3], the EnvZ osmosensor of *E. coli* ($EnvZ_{Ec}$) because of the extensive characterization of its HAMP domain within the context of the chimeric Tar-EnvZ chimeric receptors Taz and Tez[11], the nitrate-sensing histidine kinase for *E. coli* ($NarX_{Ec}$) because several HAMP domain mutations have been identified and characterized[12-14] and the aspartate chemoreceptor of *E. coli* (Tar_{Ec}) because it serves as a very well-characterized representative of the membrane-spanning chemoreceptors[15].

Experimental Design

The high-resolution three-dimensional structure of Af1503 HAMP (S278-V328)[3] served as the initial template for peptide design. Residues that formed the flexible connector (G297-A309) were excluded from the AS1- and AS2-containing peptides (AS1p-Af1503 and AS2p-Af1503). In the case of $EnvZ_{Ec}$, $NarX_{Ec}$ and Tar_{Ec}, we selected residues based on previously published[3,14,16] sequence alignments while maintaining the composition of charged and potentially helix-breaking residues. In all, 8 peptides were designed (Table 1) and synthesized (PolyPeptide Laboratories France), they were subjected to far-ultraviolet circular dicroism (Far-UV CD) and pulse field NMR (PFG-NMR) diffusion experiments. Far-UV CD measurements, using large unilamellar vesicles (LUVs) as a membrane mimetic, were employed to estimate the level of secondary structure within the peptides in the absence of lipids and to monitor induction of additional secondary structure upon mixing with LUVs. Translational diffusion experiments, employing PFG-NMR and small isotopic bicelles as a membrane mimetic, were employed to quantify the extent of peptide-lipid interaction. These results were then considered within the context of the HAMP signal transduction within SHKs and chemoreceptors.

LUVs fail to induce additional α-helical content in AS1- and AS2-containing peptides from the Af1503 and $EnvZ_{Ec}$ HAMP domains

The extent of secondary structure within the various AS1- and AS2-containing peptides was estimated using Far-UV CD spectroscopy. The 4 sets of peptides were analyzed under three different experimental conditions: a buffered aqueous solution of sodium phosphate at pH 7.2, the same buffered solution with the addition of 1 mM large unilamellar vesicles (LUVs) made of synthetic 1-palmitoyl-2-oleoyl-*sn*-glycero-3-phosphocholine (POPC, Avanti Polar Lipids), and finally, the same buffered solution with the addition of 1 mM LUVs composed of a 4:1 mixture of synthetic POPC and synthetic 1-palmitoyl-2-oleoyl-*sn*-glycero-3-phospho-(1'-rac-glycerol

(POPG, Avanti Polar Lipids). These conditions were selected to study induction of secondary structure by the presence of zwitterionic LUVs, and further induction of secondary sturcture by addition of negatively-charged phsopholipids to the LUVs, respectively. From these spectra (Figure 1), the extent of secondary structure was estimated (Figure 2).

We began by examining the peptides containing the individual helices of the Af1503 HAMP domain. In phosphate buffer, we observed more (~ 16%) α-helical content within AS2p-Af1503 than within AS1p-Af1503 (~ 4%) (Figure 2A), however within both peptides, random coil features remain dominant (Figure 1A). Furthermore, addition of LUVs consisting of either zwitterionic POPC or a 4:1 mixture of POPC/POPG that resulted in negatively-charged vesicles caused no significant induction of secondary structure (Figure 1A and Figure 2A). Likewise, peptides representing the individual helices of the EnvZ HAMP domain, namely AS1p-$EnvZ_{Ec}$ and AS2p-$EnvZ_{Ec}$, possess almost no (~ 6% and 2%, respectively) α-helical content in phosphate buffer and no striking induction was observed upon addition of either type of LUV (Figure 1B and Figure 2B). Even though the intact Af1503 HAMP domain possesses extensive secondary structure as demonstrated within the high-resolution Af1503 structure[3], our results indicate that the peptide containing AS1 is predominately unordered on its own. Because of this difference, we examined the possibility of one peptide inducing secondary structure in its cognate partner. However, the Far-UV CD spectra from all mixtures of AS1- and AS2-containing peptides exhibit the features of the average spectral properties from each peptide individually (Figure 1), indicating that they do not influence the secondary structure of their cognate partner in the absence of an intervening connector (CTR). The lack of secondary structure within AS1p- and AS2p-$EnvZ_{Ec}$ are just as striking, albeit less surprising, because an intact $EnvZ_{Ec}$ HAMP domain, containing a single point mutation (R218K) to aid in purification, was previously shown not to possess significant secondary structure[16].

LUVs induce additional α-helical content in AS1-containing peptides from the $NarX_{Ec}$ and Tar_{Ec} HAMP domains

To the contrary, addition of LUVs to the peptides representing the HAMP domains of $NarX_{Ec}$ and Tar_{Ec} induced additional α-helical content under employed experimental conditions. Upon analysis of peptides containing the individual helices of the NarX HAMP domain, AS1p-$NarX_{Ec}$ becomes significantly more α-helical (3-fold increase) upon the addition of negatively-charged LUVs (POPC:POPG 4:1) but not upon addition of zwitterionic LUVs (Figure 1C and Figure 2C). However, AS2p-$NarX_{Ec}$ remains mostly unordered under all conditions. In a similar manner, AS1p-Tar_{Ec} remains unordered in phosphate buffer, while singificant α-helical character (5-fold increase) was induced upon addition of zwitterionic LUVs, while even greater α-helical character (8-fold increase) was induced by addition of negatively-charged

LUVs (POPC:POPG 4:1). In the case of AS2p-Tar$_{Ec}$, little (~ 4%) α-helical content was observed (Figure 1D and Figure 2D). In summary, out of the 8 peptides analyzed, only AS1p-NarX$_{Ec}$, AS1p-Tar$_{Ec}$ and AS2p-Af1503 adopt extensive secondary structure in employed conditions. In the case of AS1p-NarX$_{Ec}$, this induction is only observed upon addition of negatively-charged LUVs, while with AS1p-Tar$_{Ec}$, induction of secondary sturcture is observed in the presence of either zwitterionic or negatively-charged LUVs. AS2p-Af1503 remains structured to the same extent under all experimental conditions.

AS1p-NarX$_{Ec}$, AS1p-Tar$_{Ec}$ and AS2p-Af1503 interact with phospholipid bicelles

Based on the Far-UV CD measurements described above, AS1p-NarX$_{Ec}$ and AS1p-Tar$_{Ec}$ become significantly more α-helical upon addition of zwitterionic (POPC) or both zwitterionic (POPC) and negatively-charged (POPC/POPG 4:1) LUVs, respectively (Figures 1C and 1D; Figure 2C and 2D). To employ a second assay to differentiate AS1-containing and AS2-containing peptides into different subgroups, translational diffusion measurements for all of the peptides analyzed above were performed.

These experiments were conducted with similar conditions to those used for estimation of secondary structure with slight differences. In this case, bicelles composed of different combinations of 1,2-dihexanoyl-d$_{22}$-sn-glycero-3-phosphocholine (DHPC, Avanti Polar Lipids), 1,2-dimyristoyl-d$_{54}$-sn-glycero-3-phosphocholine (DMPC, Avanti Polar Lipids) and 1,2-dimyristoyl-sn-glycero-3-phospho-(1'-rac-glycerol) (DMPG, Avanti Polar Lipids) served as membrane mimetics. The 8 peptides were analyzed in a buffered aqueous solution (D_2O) of sodium phosphate at pH 7.2, the same buffered solution with the addition of [DMPC]/[DHPC]=0.5 bicelles, and finally, the same buffered solution with [DMPC/DMPG 4:1]/[DHPC] bicelles. Here, we assume that all DMPC and DMPG molecules are located within the bicelles, thus allowing us to assume that the average diffusion coefficient of DMPC and DMPG is equivalent to that of the bicelle[17].

Starting with the AS1 peptides, the translational diffusion of AS1p-NarX$_{Ec}$ in phosphate buffer is described by a diffusion coefficient (D) of $1.5 \cdot 10^{-10}$ m^2/s, which is consistent with the translational motion of a peptide of this size[18]. This is reduced to $0.40 \cdot 10^{-10}$ m^2/s in the presence of [DMPC]/[DHPC] bicelles and to $0.35 \cdot 10^{-10}$ m^2/s in the presence of bicelles composed of [DMPC/DMPG 4:1]/[DHPC], which are both comparable to the coefficients for bicelles alone ($0.38 \cdot 10^{-10}$ m^2/s and $0.35 \cdot 10^{-10}$ m^2/s, respectively). AS1p-Tar$_{Ec}$ diffuses at $1.4 \cdot 10^{-10}$ m^2/s in phosphate buffer, and this is also reduced to $0.38 \cdot 10^{-10}$ m^2/s in the presence of [DMPC]/[DHPC] bicelles and to $0.36 \cdot 10^{-10}$ m^2/s in the presence of bicelles composed of [DMPC/DMPG 4:1]/[DHPC]. If a two-state exchange process is assumed between the bicelle-bound peptide and the peptide in solution, it is possible to estimate the extent of interaction by using equation 1[17].

$$x \cdot D_{DMPC\,/\,DMPG} + (1-x) \cdot D_{free} = D_{bound} \qquad [1]$$

where $D_{DMPC/DMPG}$ is the diffusion coefficient of the bicelle, D_{free} is the diffusion coefficient of the peptide in buffer, D_{bound} is the diffusion coefficient of the peptide in the bicelle-solution and x is the amount of peptide that are bound to the bicelle. Based on these calculations, all of the AS1p-$NarX_{Ec}$, AS1p-Tar_{Ec} or AS2p-Af1503 in the samples is bound to the bicelles under our experimental conditions. AS2p-Af1503 has a diffusion coefficient of $1.6 \cdot 10^{-10}$ m^2/s in phosphate buffer, which is reduced to $0.39 \cdot 10^{-10}$ m^2/s in the presence [DMPC]/[DHPC] bicelles and $0.40 \cdot 10^{-10}$ m^2/s in the presence of bicelles composed of [DMPC/DMPG 4:1]/[DHPC]. For the other AS1- and AS2-containing peptides examined, all show a slight reduction in the diffusion coefficient upon addition of bicelles, which suggests some proportion of the peptide is interacting with the bicelles, but none were found to completely bind to bicelles, as is the case with AS1p-$NarX_{Ec}$, AS1p-Tar_{Ec} or AS2p-Af1503 (Table 2).

Differentiation of HAMP domains into subgroups based on membrane-induced characteristics

A wide variety of periplasmic stimulus-sensing domains are employed within prokaryotic membrane-spanning receptors. HAMP domains usually reside between these domains and the cytoplasmic domain responsible for signal generation[2], therefore, they must possess the ability to process different types of conformational input. We propose that the four HAMP domains we examined can be classified into two subgroups based on the ability of membrane mimetics to induce additional α-helicity in their respective AS1-containing peptides and for their degree of interactions with various membrane mimetics.

The first group contains HAMP domains ($NarX_{Ec}$ and Tar_{Ec}) whose AS1-containing peptides become more α-helical upon addition of LUVs (Figures 1C and 1D; Figure 2C and 2D) and that were found to interact with bicelles (Table 2). The similarity in these results may not be surprising when one considers the evidence that exists suggesting that they share a common mechanism of transmembrane communication. In the case of Tar_{Ec}, and other related chemoreceptors, a wide variety of methodological approaches[15] have demonstrated that a single extended helix consisting of the final C-terminal helix of the periplasmic four-helix bundle (PD4) and the second transmembrane helix (TM2) is slightly displaced (~ 1-2 Å) toward the cytoplasm upon binding of aspartate to the periplasmic domain. In the case of $NarX_{Ec}$, recent high-resolution three-dimensional structures of a soluble form of the periplasmic domain, in the presence and in the absence of nitrate, have been determined[19]. Superimposition of these two structures demonstrates a slight (~ 1 Å) displacement downward, or toward the cytoplasm within the intact receptor, of the N-terminal helices within the four-helix bundles (PD1 and PD1') relative to the C-terminal helices (PD4 and PD4'). However, it should be noted that this structural

determination was carried out it in the absence of detergent or other membrane mimetic, and that when the intact receptor is embedded within the cytoplasmic membrane, that PD4-TM2 and PD4'-TM2' may slide upward relative to the plane of the membrane and to PD1-TM1 and/or PD1'-TM1'. In addition, the functionality of a $NarX_{Ec}$-Tar_{Ec} chimera Nart[20] supports the notion that transmembrane communication occurs through PD4-TM2 and/or PD4'-TM2' within both receptors. Therefore, we suggest that a correlation exists between this subgroup of HAMP domains and receptors that possess periplasmic four-helix bundles and presumably transmit the presence of stimulus across the membrane via piston-type displacements of TM2. Furthermore, we propose that within this subgroup of HAMP domains, a slight displacement TM2 displacement could alter the proximity of AS1 to the inner leaflet of the membrane, thereby controlling its propensity for α-helix formation (Figure 3). If the energetic landscape of possible HAMP configurations is such that the energy required to interconvert between the localized minima representing the opposite signaling configurations remains low as has been proposed[3,7-10], then changes in the α-helicity of AS1 could serve as a conduit for converting piston-type displacements into altered downstream conformational dynamics (Figure 3). Within the context of the proposed models for HAMP domain signal transduction, changes in the α-helicity of AS1 could be responsible modulating contact between individual helices to facilitate a concerted rotation of the four helices as suggested within the "gearbox" model[3], for modulating the rigidity required within the "pivoting" model[8], or could contribute to the overall stability within the context of the "dynamic bundle" model[9]. In addition, the alterations observed in density maps within the "compact" and "expanded" forms of the HAMP domains within trimers-of-dimers[10] could be facilitated by modulation of AS1 α-helicity.

Members of the second subgroup of HAMP domains possess a greatly reduced effect of helical induction in AS1 by the membrane mimetics and a reduced interaction with bicelles, when compared to the members of the first subgroup. The intact receptors containing the HAMP domains we analyzed here, namely Af1503 and $EnvZ_{Ec}$, do not possess a periplasmic four-helix bundle, based on secondary structure prediction with JPRED3[21] or based on biophysical analyses, respectively[22]. Furthermore, no evidence exists for piston-type displacements by the TM2s within these receptors. Therefore, we propose that alternate membrane-independent forms of signal transduction employed are by HAMP domains within these receptors.

In conclusion, we believe that these results represent an examination of the potential contributions by biological membranes to the conformational dynamics of membrane-proximal HAMP domains. Furthermore, within one subset of HAMP domains ($NarX_{Ec}$ and Tar_{Ec}), we hypothesize that modulation of these contributions could serve as a central component of transmembrane communication by these receptors containing this subset of HAMP domains.

Acknowledgements

This work was supported by the Swedish Research Council and the Centre for Biomembrane Research. R.D. was supported by a Ruth L. Kirschstein National Research Service Award from the National Institutes of Health (F32-AI075773).

References

1. Aravind, L. & Ponting, C. P. (1999). The cytoplasmic helical linker domain of receptor histidine kinase and methyl-accepting proteins is common to many prokaryotic signalling proteins. *FEMS Microbiol Lett* **176**, 111-6.
2. Ulrich, L. E. & Zhulin, I. B. (2005). Four-helix bundle: a ubiquitous sensory module in prokaryotic signal transduction. *Bioinformatics* **21 Suppl 3**, iii45-8.
3. Hulko, M., Berndt, F., Gruber, M., Linder, J. U., Truffault, V., Schultz, A., Martin, J., Schultz, J. E., Lupas, A. N. & Coles, M. (2006). The HAMP domain structure implies helix rotation in transmembrane signaling. *Cell* **126**, 929-40.
4. Ames, P. & Parkinson, J. S. (1988). Transmembrane signaling by bacterial chemoreceptors: E. coli transducers with locked signal output. *Cell* **55**, 817-26.
5. Butler, S. L. & Falke, J. J. (1998). Cysteine and disulfide scanning reveals two amphiphilic helices in the linker region of the aspartate chemoreceptor. *Biochemistry* **37**, 10746-56.
6. Williams, S. B. & Stewart, V. (1999). Functional similarities among two-component sensors and methyl-accepting chemotaxis proteins suggest a role for linker region amphipathic helices in transmembrane signal transduction. *Mol Microbiol* **33**, 1093-102.
7. Watts, K. J., Johnson, M. S. & Taylor, B. L. (2008). Structure-function relationships in the HAMP and proximal signaling domains of the aerotaxis receptor Aer. *J Bacteriol* **190**, 2118-27.
8. Swain, K. E. & Falke, J. J. (2007). Structure of the conserved HAMP domain in an intact, membrane-bound chemoreceptor: a disulfide mapping study. *Biochemistry* **46**, 13684-95.
9. Zhou, Q., Ames, P. & Parkinson, J. S. (2009). Mutational analyses of HAMP helices suggest a dynamic bundle model of input-output signalling in chemoreceptors. *Mol Microbiol* **73**, 801-14.
10. Khursigara, C. M., Wu, X., Zhang, P., Lefman, J. & Subramaniam, S. (2008). Role of HAMP domains in chemotaxis signaling by bacterial chemoreceptors. *Proc Natl Acad Sci U S A* **105**, 16555-60.
11. Yoshida, T., Phadtare, S. & Inouye, M. (2007). The design and development of Tar-EnvZ chimeric receptors. *Methods Enzymol* **423**, 166-83.
12. Kalman, L. V. & Gunsalus, R. P. (1990). Nitrate- and molybdenum-independent signal transduction mutations in narX that alter regulation of anaerobic respiratory genes in Escherichia coli. *J Bacteriol* **172**, 7049-56.
13. Collins, L. A., Egan, S. M. & Stewart, V. (1992). Mutational analysis reveals functional similarity between NARX, a nitrate sensor in Escherichia coli K-12, and the methyl-accepting chemotaxis proteins. *J Bacteriol* **174**, 3667-75.
14. Appleman, J. A. & Stewart, V. (2003). Mutational analysis of a conserved signal-transducing element: the HAMP linker of the Escherichia coli nitrate sensor NarX. *J Bacteriol* **185**, 89-97.
15. Falke, J. J. & Hazelbauer, G. L. (2001). Transmembrane signaling in bacterial chemoreceptors. *Trends Biochem Sci* **26**, 257-65.
16. Kishii, R., Falzon, L., Yoshida, T., Kobayashi, H. & Inouye, M. (2007). Structural and functional studies of the HAMP domain of EnvZ, an osmosensing transmembrane histidine kinase in Escherichia coli. *J Biol Chem* **282**, 26401-8.
17. Andersson, A., Almqvist, J., Hagn, F. & Maler, L. (2004). Diffusion and dynamics of penetratin in different membrane mimicking media. *Biochim Biophys Acta* **1661**, 18-25.

18. Danielsson, J., Jarvet, J., Damberg, P. and Gräslund, A. (2002). Translational diffusion measured by PFG-NMR on full length and fragments of the Alzheimer Aβ(1-40) peptide. Determination of hydrodynamic radii of random coil peptides of varying length. . *Magn. Reson. Chem.* **40**, S89-S97.
19. Cheung, J. & Hendrickson, W. A. (2009). Structural analysis of ligand stimulation of the histidine kinase NarX. *Structure* **17**, 190-201.
20. Ward, S. M., Delgado, A., Gunsalus, R. P. & Manson, M. D. (2002). A NarX-Tar chimera mediates repellent chemotaxis to nitrate and nitrite. *Mol Microbiol* **44**, 709-19.
21. Cole, C., Barber, J. D. & Barton, G. J. (2008). The Jpred 3 secondary structure prediction server. *Nucleic Acids Res* **36**, W197-201.
22. Egger, L. A. & Inouye, M. (1997). Purification and characterization of the periplasmic domain of EnvZ osmosensor in Escherichia coli. *Biochem Biophys Res Commun* **231**, 68-72.
23. Whitmore, L. & Wallace, B. A. (2004). DICHROWEB, an online server for protein secondary structure analyses from circular dichroism spectroscopic data. *Nucleic Acids Res* **32**, W668-73.
24. Provencher, S. W. & Glockner, J. (1981). Estimation of globular protein secondary structure from circular dichroism. *Biochemistry* **20**, 33-7.
25. Callaghan, P. T., Komlosh, M. E. & Nyden, M. (1998). High magnetic field gradient PGSE NMR in the presence of a large polarizing field. *J Magn Reson* **133**, 177-82.
26. Stejskal, E. O., & Tanner, J.E. (1965). Spin Diffusion Measurements: Spin Echoes in the Presence of a Time-Dependent Field Gradient. *J. Chem. Phys.* **42**, 288-292.
27. Von Meerwall, E. K., M. (1989). Effect of Residual Field Gradients on Pulsed Gradient NMR Diffusion Measurments. *J. Magn. Reson.* **83**, 309-323.
28. Damberg, P., Jarvet, J. & Graslund, A. (2001). Accurate measurement of translational diffusion coefficients: a practical method to account for nonlinear gradients. *J Magn Reson* **148**, 343-8.
29. Longsworth, L. G. (1960). The Mutual Diffusion of Light and Heavy Water. *J. Phys. Chem.* **64**, 1914-1917.

Figure legends

Figure 1. Far-UV CD spectra of the various AS1- and AS2-containing peptides examined during this study. The peptides analyzed are constituents of the various HAMP domains of (A) Af1503, (B) $EnvZ_{Ec}$, (C) $NarX_{Ec}$, and (D) Tar_{Ec}. Samples contain a final concentration of 50 μM peptide (AS1, AS2, or a 1:1 mix of AS1 and AS2), 50 mM soudium phosphate pH 7.2 (left panel) and 1 mM POPC (middle panel) or 1mM POPC/POPG 4:1 (right panel). Measurements were acquired on a Chirascan CD spectrometer with a 1 mm quartz cell at 298 K. Wavelengths ranging from 190 to 260 nm were measured with a 0.5 nm step resolution. Spectra were collected and averaged over ten measurements with the appropriate background values subtracted.

Figure 2. Estimation of the extent of secondary structure from Far-UV CD spectra. The spectra were further analyzed with Dichroweb[23] using the CONTIN method[24] with reference set 7, optimized for the range 190-240 nm. The fraction of helix, strand, turns and unordered secondary structure is shown for the 8 peptides derived from (A) Af1503, (B) $EnvZ_{Ec}$, (C) $NarX_{Ec}$, and (D) Tar_{Ec} in 50 mM NaPi buffer pH 7.2 (in white), 50 mM NaPi with 1 mM POPC (in light grey) and 50 mM NaPi with 1mM POPC/POPG 4:1 (in dark grey). Focusing on the helix content of the peptides, a structure induction in AS1p-Tar_{Ec} is seen upon addition of POPC (~ 5-fold) and POPC/POPG (~ 8-fold). Similarly, a helical structure induction of AS1p-$NarX_{Ec}$ (~ 3-fold) is seen upon addition of POPC/POPG. AS2p-Af1503, on the other hand, exhibits 16% helical content in all three conditions.

Figure 3. Piston-type displacements of TM2 may reduce membrane-based influences within AS1. Tar_{Ec}[15] and $NarX_{Ec}$[20] have been suggested to participate in transmembrane communication by displacements of TM2. Our results suggest that various membrane mimetics alter the α-helicity of AS1-containing peptides from HAMP domains within these receptors. Therefore, we hypothesize that one possibility for converting a piston-type displacement of TM2 into signal transduction within these HAMP domains is by reducing the contributions of the inner leaflet of the cell membrane to the α-helicity of AS1.

Table legends

Table 1. Residues selected for AS1- and AS2-containing peptides used in this study. Peptides were obtained (PolyPeptide Laboratories France) and used as received.

Table 2. Diffusion coefficients for the AS1- and AS2-containing peptides employed in this study. PFG-NMR samples of 500 μM AS1p or AS2p in 50 mM sodium phosphate buffer (pH 7.2) was prepared to measure the diffusion coefficients of the peptides in buffer, D_{free}. Bicelle samples were prepared by dissolving peptide in 150 mM [DMPC]/[DHPC] or 150 mM [DMPC/DMPG 4:1]/[DHPC], respectively, in 50 mM sodium phosphate buffer (pH 7.2). The q-ratio (long-chained phospholipids)/(short-chained phospholipids) was maintained at 0.5. All samples were dissolved in D_2O. Translational diffusion experiments were performed at 298 K on a Bruker Avance spectrometer, equipped with a triple resonance probe head and operating at a ^1H frequency of 600 MHz. A standard sample of 0.01% H_2O in D_2O and 1 mg/ml $GdCl_3$ was used for calibration, to avoid radiation damping. Diffusion coefficients were measured using a modified Stejskal-Tanner spin-echo experiment[25-27] using a fixed diffusion time and gradient length and with a gradient strength varying linearly over 32 steps. The linearity of the gradient was calibrated as described previously[28]. The diffusion coefficient for HDO was measured and divided by the standard diffusion of HDO in D_2O ($1.9\ 10^{-9}$)[29]. This quotient was then multiplied to all measured diffusion constants, to correct for viscosity differences induced by the sample.

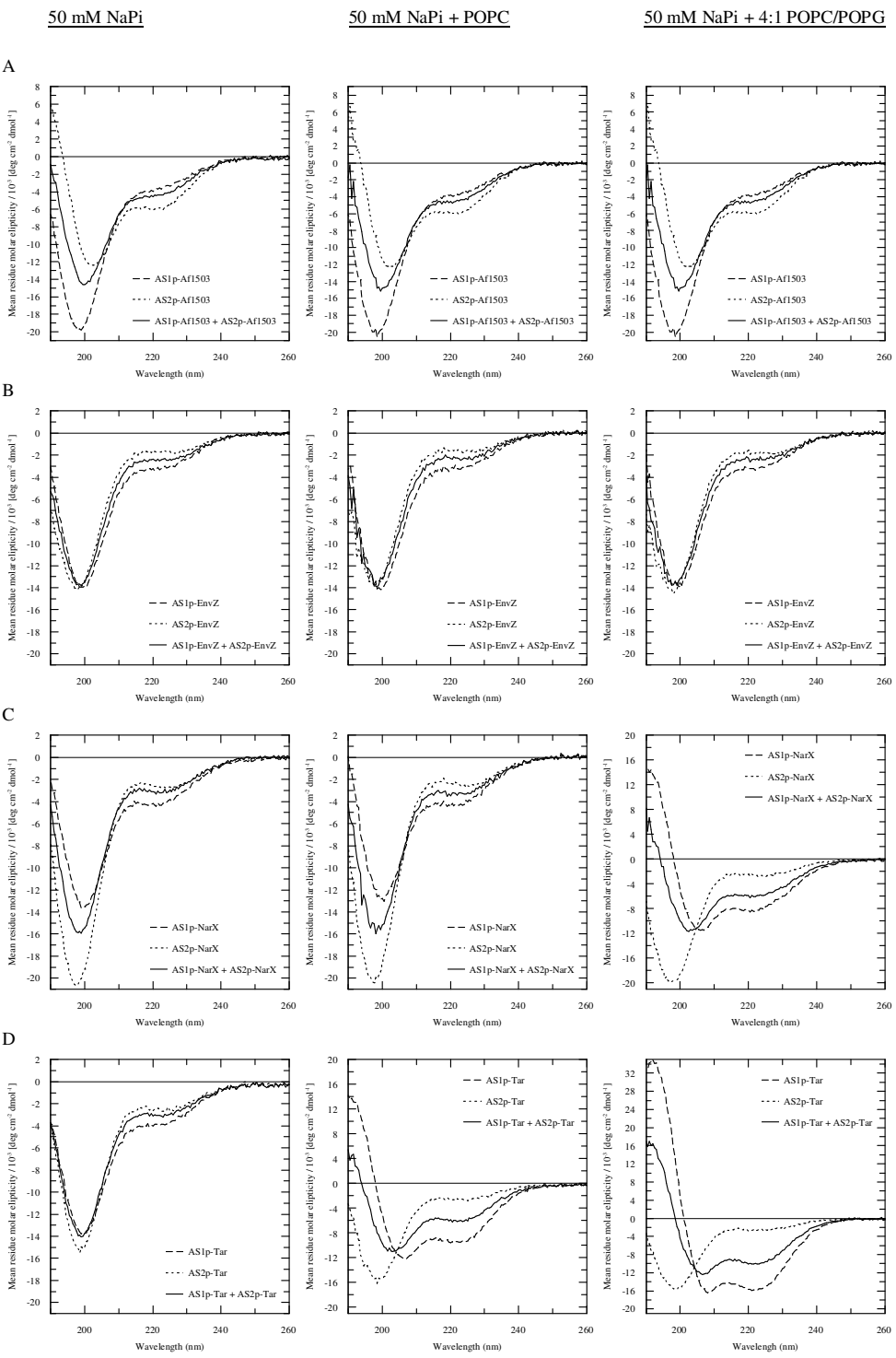
50 mM NaPi
50 mM NaPi + POPC
50 mM NaPi + 4:1 POPC/POPG
A
B
C
D
Mean residue molar ellipticity / 10³ [deg cm² dmol⁻¹]
Wavelength (nm)
AS1p-Af1503
AS2p-Af1503
AS1p-Af1503 + AS2p-Af1503
AS1p-EnvZ
AS2p-EnvZ
AS1p-EnvZ + AS2p-EnvZ
AS1p-NarX
AS2p-NarX
AS1p-NarX + AS2p-NarX
AS1p-Tar
AS2p-Tar
AS1p-Tar + AS2p-Tar

Figure 1.

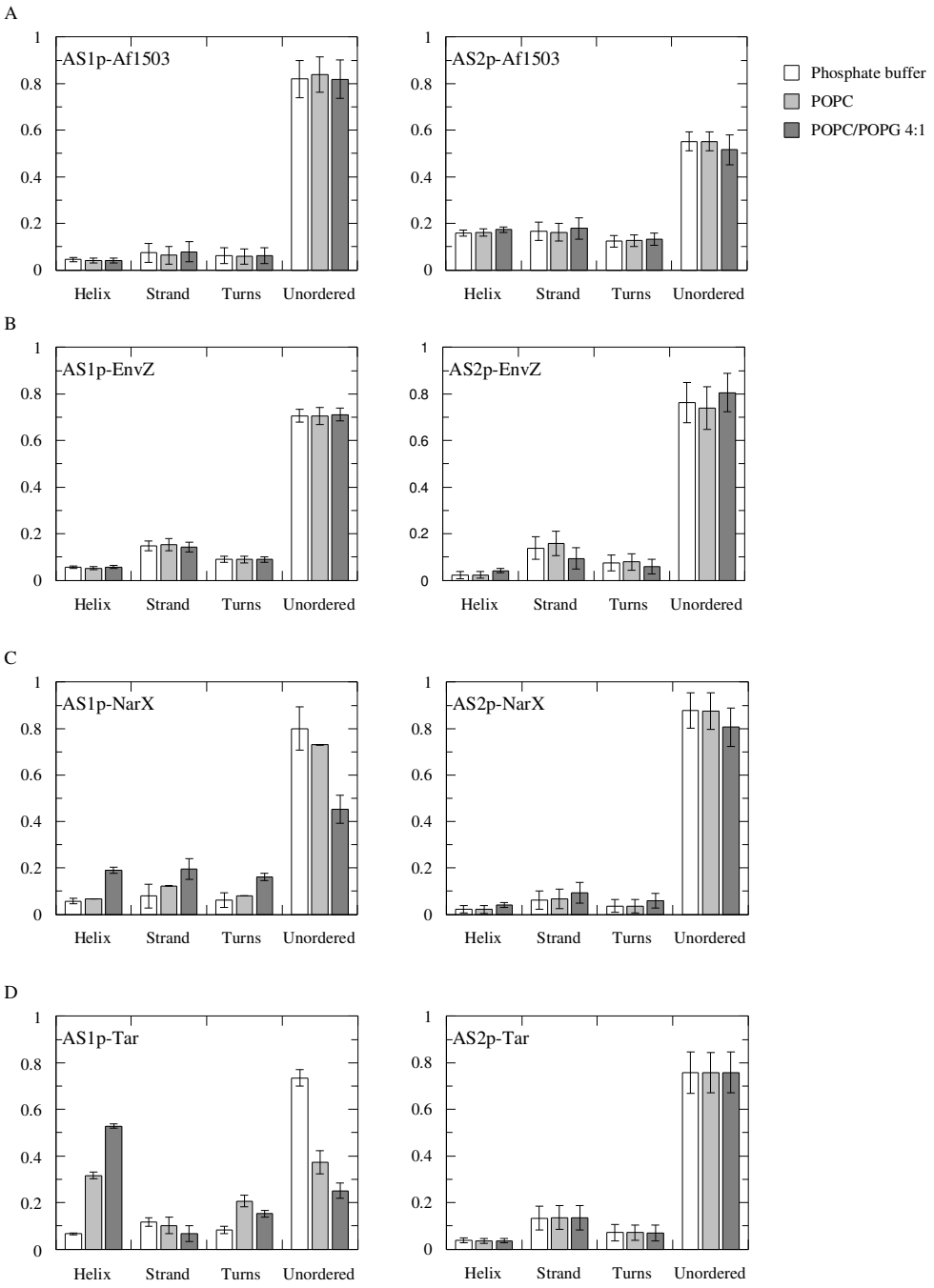
A
AS1p-Af1503
AS2p-Af1503
B
AS1p-EnvZ
AS2p-EnvZ
C
AS1p-NarX
AS2p-NarX
D
AS1p-Tar
AS2p-Tar
Phosphate buffer
POPC
POPC/POPG 4:1
Helix
Strand
Turns
Unordered
0
0.2
0.4
0.6
0.8
1

Figure 2.

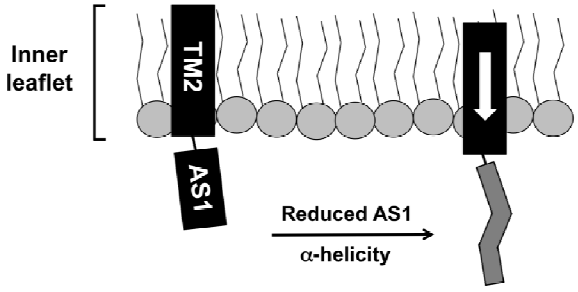

Figure 3.

Table 1.

Receptor[a]	GI[b]	Peptide	Sequence
Af1503 (278-296)	2649073	AS1p-Af1503	STITRPIIELSNTADKIAE
Af1503 (310-328)	2649073	AS2p-Af1503	DEIGILAKSIERLRRSLKV
$EnvZ_{Ec}$ (180-198)	119394	AS1p-$EnvZ_{Ec}$	RIQNRPLVDLEHAALQVGK
$EnvZ_{Ec}$ (211-229)	119394	AS2p-$EnvZ_{Ec}$	SEVRSVTRAFNHMAAGVKQ
$NarX_{Ec}$ (177-195)	127840	AS1p-$NarX_{Ec}$	RLLQPWRQLLAMASAVSHR
$NarX_{Ec}$ (208-226)	127840	AS2p-$NarX_{Ec}$	EMAMLGTALNNMSAELAES
Tar_{Ec} (214-232)	1788195	AS1p-Tar_{Ec}	RMLLTPLAKIIAHIREIAG
Tar_{Ec} (246-263)	1788195	AS2p-Tar_{Ec}	EMGDLAQSVSHMQRSLTD

[a] The receptor that served a the source of AS1- and AS2-containing peptides. The residue numbers, within the context of the primary sequence of the intact receptor are provided in parentheses
[b] The "GenInfo Identifier" sequence identification number

Table 2.

	Diffusion coefficient (10^{-10} m^2/s)						
	NaPi	DMPC/DHPC			(DMPC/DMPG 4:1)/DHPC		
Peptide	D_{free}	D_{bound}	D_{DMPC}	x (%)	D_{bound}	D_{DMPC}	x (%)
AS1p-Af1503	1.6 ± 0.07	1.2 ± 0.07	0.38 ± 0.01	36	0.96 ± 0.1	0.36 ± 0.01	52
AS2p-Af1503	1.6 ± 0.02	0.39 ± 0.01	0.37 ± 0.01	98	0.40 ± 0.01	0.37 ± 0.01	98
AS1p-$EnvZ_{Ec}$	1.6 ± 0.05	1.2 ± 0.04	0.38± 0.02	36	1.1 ± 0.04	0.39 ± 0.01	43
AS2p-$EnvZ_{Ec}$	1.6 ± 0.04	1.0 ± 0.05	0.35 ± 0.01	48	1.1 ± 0.03	0.37 ± 0.01	40
AS1p-$NarX_{Ec}$	1.5 ± 0.05	0.40 ± 0.01	0.38 ± 0.01	98	0.35 ± 0.01	0.36 ± 0.01	100
AS2p-$NarX_{Ec}$	1.6 ± 0.04	1.0 ± 0.02	0.37 ± 0.01	49	0.92 ± 0.02	0.37 ± 0.01	58
AS1p-Tar_{Ec}	1.4 ± 0.04	0.38 ± 0.01	0.37 ± 0.01	99	0.35 ± 0.01	0.36 ± 0.01	100
AS2p-Tar_{Ec}	1.7 ± 0.06	1.2 ± 0.04	0.38 ± 0.01	42	1.2 ± 0.05	0.37 ± 0.01	40